ARMY RESEARCH LABORATORY

Characterization of Corrosion on Outdoor-Exposed Aluminum Metal-Matrix Composites as a Function of Reinforcement Specie and Volume Fraction

by Ralph P. I. Adler, Daniel J. Snoha, George Hawthorn, and Lloyd H. Hihara

ARL-TR-4372 **February 2008**

NOTICES

Disclaimers

The findings in this report are not to be construed as an official Department of the Army position unless so designated by other authorized documents.

Citation of manufacturer's or trade names does not constitute an official endorsement or approval of the use thereof.

Destroy this report when it is no longer needed. Do not return it to the originator.

Army Research Laboratory
Aberdeen Proving Ground, MD 21005-5069

ARL-TR-4372 **February 2008**

Characterization of Corrosion on Outdoor-Exposed Aluminum Metal-Matrix Composites as a Function of Reinforcement Specie and Volume Fraction

Ralph P. I. Adler and Daniel J. Snoha
Weapons and Materials Research Directorate, ARL

George Hawthorn and Lloyd H. Hihara
University of Hawaii

REPORT DOCUMENTATION PAGE

Form Approved
OMB No. 0704-0188

1. REPORT DATE *(DD-MM-YYYY)*	2. REPORT TYPE	3. DATES COVERED (From - To)
February 2008	Final	June 2004–November 2006

4. TITLE AND SUBTITLE
Characterization of Corrosion on Outdoor-Exposed Aluminum Metal-Matrix Composites as a Function of Reinforcement Specie and Volume Fraction

5a. CONTRACT NUMBER

5b. GRANT NUMBER

5c. PROGRAM ELEMENT NUMBER

6. AUTHOR(S)
Ralph P. I. Adler, Daniel J. Snoha, George Hawthorn,* and Lloyd H. Hihara*

5d. PROJECT NUMBER
M089 589131

5e. TASK NUMBER

5f. WORK UNIT NUMBER

7. PERFORMING ORGANIZATION NAME(S) AND ADDRESS(ES)
U.S. Army Research Laboratory
ATTN: AMSRD-ARL-WM-MC
Aberdeen Proving Ground, MD 21005-5069

8. PERFORMING ORGANIZATION REPORT NUMBER
ARL-TR-4372

9. SPONSORING/MONITORING AGENCY NAME(S) AND ADDRESS(ES)

10. SPONSOR/MONITOR'S ACRONYM(S)

11. SPONSOR/MONITOR'S REPORT NUMBER(S)

12. DISTRIBUTION/AVAILABILITY STATEMENT
Approved for public release; distribution is unlimited.

13. SUPPLEMENTARY NOTES
*Hawaii Corrosion Laboratory, Department of Mechanical Engineering, University of Hawaii at Manoa, Honolulu, HI 96826

14. ABSTRACT
The Hawaii Corrosion Laboratory and the U.S. Army Research Laboratory collaborated to prepare, environmentally expose for up to 2 years, and evaluate multivariant sets of metal matrix composites (MMCs). The experimental matrix involved variations in particulate volume-percent and particulate reinforcement specie (higher purity green and less-pure black silicon carbide, boron carbide, and alumina). The specific objective of this study was to determine, mainly using x-ray powder diffractometry, how observed gravimetric variations in corrosion behavior of these sets of MMCs (differentiated by four kinds of reinforcing agents with some variations in volume-percent), after relatively heavy-rainfall outdoor exposures in Hawaii, could be related to the crystallographic and morphological characteristics of the resulting corrosion products. Compared to the monolithic aluminum control specimens, the measured corrosion rates for these MMCs were considerably accelerated (by at least an order of magnitude) by the presence and relative amount of these second-phase particulates. The increased kinetics found for these MMCs were nominally proportional to the volume fraction of the particulate phase. Other differentials in gravimetric corrosion rates and corrosion product characteristics were related to the type of reinforcement phase present.

15. SUBJECT TERMS
corrosion, aluminum metal-matrix composites, silicon carbide, boron carbide, alumina, Bayerite

16. SECURITY CLASSIFICATION OF:			17. LIMITATION OF ABSTRACT	18. NUMBER OF PAGES	19a. NAME OF RESPONSIBLE PERSON
a. REPORT	b. ABSTRACT	c. THIS PAGE			Ralph P. I. Adler
UNCLASSIFIED	UNCLASSIFIED	UNCLASSIFIED	UL	52	19b. TELEPHONE NUMBER (*Include area code*) (410) 306-0826

Contents

List of Figures

List of Tables

Acknowledgments

The authors are grateful for the support from the Pacific Rim Corrosion Research Program under U.S. Army contract DAAE30-03-C-1071 administered through the Army Corrosion Office (by Robert Zanowicz, John Theis, and Dr. Joseph Argento), located at Picatinny Arsenal, NJ. We also thank our colleagues at the Hawaii Corrosion Laboratory and the U.S. Army Research Laboratory for their administrative and technical support.

INTENTIONALLY LEFT BLANK.

1. Introduction

The promising metallurgical concept of incorporating stiff ceramic fiber as reinforcements into metallic matrices to produce metal-matrix composites (MMCs) with enhanced properties relative to the monolithic metal has been well demonstrated by academia and industry. However, there has been relatively less concern that the presence of such second (reinforcing) phases could have some compositional (due to electrochemical differences), physical (e.g., large differences in electrical resistivity among the ceramic phases, see table 1), and microstructural effects on corrosion phenomena and associated kinetics.

Table 1. Resistivities of selected materials.

Material	Resistivity (Ω cm)	Temperature (°C)	Notes	Reference
B_4C	10^{1}	—	Pure	(*1*)
SiC	10^{-5}–10^{13}	—	Dependant on purity	(*2*)
Al_2O_3	$>10^{14}$	30	99.7%	(*3*)
TiO_2	10^{13}–10^{18}	25	99.6%	(*4*)

Numerous MMC components with continuous or discontinuous reinforcing fibers and particulates (silicon carbide [SiC], boron carbide [B_4C], and alumina [Al_2O_3]), primarily with aluminum alloy (Al) matrices, are already being produced for various applications (*5*). Al-SiC MMCs are generally used in structural and electronic applications, while Al-B_4C MMCs and Al-Al_2O_3 MMCs are generally used in structural applications. Each type of reinforcement constituent possesses certain advantages and disadvantages. Of these Al MMCs, those with SiC reinforcements are the most prevalent. In structural applications, low-purity black SiC is used at loadings between 15 and 25 volume-percent. In electronic-packaging applications (*5*), the major function of the SiC, whose reinforcement content ranges from ~30–55 volume-percent, is to reduce the MMC coefficient of thermal expansion to values closer to those of electronic-component materials such as gallium arsenide. In electronic-grade MMCs, high-purity green SiC is preferred for its high thermal conductivity. The green SiC also possesses high electrical resistivity and should be less likely to promote any galvanic corrosion of the aluminum matrix as compared to black SiC that, because it is less pure, has a lower resistivity. B_4C has some advantages over SiC in that it is 20% lighter, improves MMC weldability, and is good for neutron shielding (*5*). The relatively low electrical resistivity (*6*) of B_4C (10^{-1}–10^{1} Ω cm) may promote galvanic corrosion in MMCs. Al_2O_3 reinforcements have the advantage of being an insulator ($>10^{14}$ Ω cm) and, thus, should not promote galvanic corrosion with the aluminum matrix. However, the density of Al_2O_3 (*6*) is more than 20% higher than that of SiC, resulting in a heavier MMC for the same volume-fraction reinforcement.

The primary concern, with respect to the corrosion durability of Al MMCs, is that galvanic corrosion may occur when the incorporated particles or fibers are conductive or semiconductive (*7, 8*). The galvanic effect of a conductor such as graphite has been generally accepted; whereas, galvanic effects of the nonmetallic components such as SiC, a semiconductor with resistivities ranging from 10^{-5} to 10^{13} Ω cm, depending on its purity (*2, 9*), are in question. Theoretically, when aluminum is coupled with an insulating component such as Al_2O_3, there should be no galvanic effects. B_4C has a relatively low resistivity (~1 Ω cm), and, therefore, galvanic coupling is likely. For the SiC-reinforced MMCs, the current Hawaii Corrosion Laboratory (HCL) scanning vibrating electrode technique and scanning ion-selective electrode technique results also indicate a galvanic effect (*10*). First, there are similar characteristics on the current density maps and pH profiles over the localized corrosion regions that formed on 20-volume-percent B_4C and 20-volume-percent SiC Al MMCs. Second, the corrosion behavior of 20-volume-percent Al_2O_3 Al MMC is different from that of the 20-volume-percent B_4C and 20-volume-percent SiCAl MMCs. Third, the extent of corrosion of 20-volume-percent SiC-reinforced Al MMC was lower than that of the 20-volume-percent B_4C-reinforced Al MMC. That the extent of corrosion of these three MMCs decreased with increasing reinforcement resistivities indicates that galvanic effects accelerated the corrosion process.

Accordingly, the specific objective of this study was to determine the impact of the relative volume fraction and reinforcement specie on the bulk corrosion rates of discontinuously reinforced Al MMCs relative to a comparable monolithic aluminum alloy after outdoor exposures at the highest rainfall (HCL test site at the Lyon Arboretum on Oahu). Further characterizations of crystallographic and morphological features of the resulting corrosion products, acquired mainly using x-ray powder diffractometry techniques, were used to obtain correlations with the gravimetric results.

2. Experimental Materials and Sample Preparation

2.1 MMC Specimens

The discontinuously reinforced aluminum MMCs were fabricated by DWA Aluminum Composites (Chatsworth, CA) using nominally identical processing and thermomechanical histories to avoid differences in corrosion behavior associated with processing inconsistencies. Each custom MMC lot was fabricated using DWA's proprietary powder metallurgy and hot-pressing processing operation forming nominally 3.7-in-diameter billets that were then heat treated to the T6 condition. The chemical composition of the 6092 aluminum alloy matrix is listed in table 2. Corrosion disk samples, nominally 0.1 in thick, were cut from the billet by electrical discharge machining (EDM) followed by abrasive grit-blasting to remove the recast layer induced by EDM thermal effects.

Table 2. Composition of 6061 and 6092 aluminum alloys.

Alloy	Solute Concentrations (Volume-Percent Solute by Element)							
	Si	Fe	Cu	Mn	Mg	Cr	Zn	Ti
6061 Al	0.4–0.8	0.7	0.15–0.4	0.15	0.8–1.2	0.04–0.35	0.25	0.15
6092 Al	0.75	0.09	0.83	NA	1.05	NA	NA	0.05

Note: NA = not applicable.

The MMC particulate reinforcements were green and black SiC, B_4C, and Al_2O_3. The black SiC volume fractions were 5, 10, 20, 40, and 50 volume-percent, the green SiC was 50 volume-percent, and the B_4C and Al_2O_3 were 20 volume percent. However, only the 20- and 50-volume-percent black SiC samples were selected for this study to determine the effect of SiC volume fraction on corrosion behavior. The 20-volume-percent series of black SiC, B_4C, and Al_2O_3 MMCs compared the effect of reinforcement resistivity on corrosion behavior; likewise for the MMCs with 50-volume-percent black and green SiC.

2.2 Monolithic 6061-T6 Aluminum Alloy Control Specimens

The control samples were nominally 2- × 2- × 0.125-in coupons machined from wrought sheet stock. The 6061 aluminum alloy composition, listed in table 2, was a close match to the powder-metallurgy-produced 6092 aluminum alloy's composition.

3. Experimental Procedures

3.1 Outdoor-Exposure Corrosion Studies

3.1.1 Test Site, Corrosion-Exposure Racks, and Gravimetric Measurements

MMC and control specimens were exposed to a heavy-rainfall atmospheric test site located in the Lyon Arboretum on the island of Oahu. The Lyon Arboretum site is on University of Hawaii (UH) property. Test-site maintenance (including changing chloride candles, downloading weather data, photography, and/or retrieving specimens) was performed on a monthly basis.

Test racks were designed and constructed using 316 stainless steel and Trex* materials. Trex is a wood-like composite made from recycled wood chips and recycled polyethylene. Test racks on UH had Trex slats on a stainless-steel frame. For this corrosion study, the MMC and monolithic specimens were exposed at 30° from the horizontal, and each specimen was secured with three nylon insulators.

* Trex is a registered trademark of Trex Company, Inc.

3.1.2 Outdoor-Exposure Specimens

Each MMC disk (0.1 in thick and ranging in diameter from 3.56 to 3.75 in) was stamped with an alphanumeric code using a Telisis Benchmark 320 pin-stamping system. The disks were washed in acetone, followed by ultrasonic cleaning in deionized water. After drying, each specimen was weighed on a Mettler AE163 electronic balance. The initial weight of each specimen was measured in grams to four decimal places. Figure 1 shows a typical arrangement of the MMC specimens on a test rack.

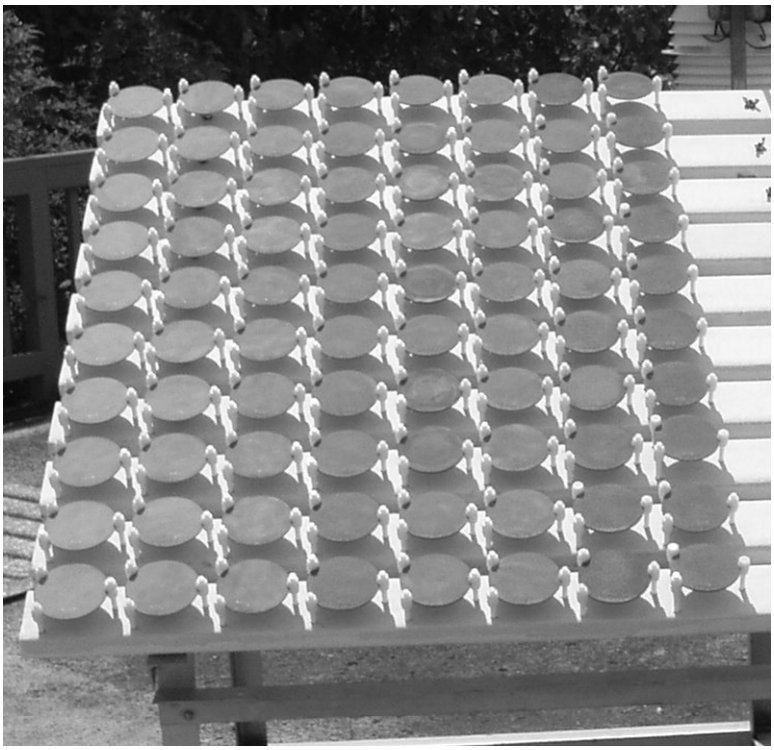

Figure 1. Typical arrangement of Al MMCs on outdoor-exposure rack at test site.

Samples of the eight lots of MMCs were arranged in eight columns of 10 rows, where each column contained the same type of MMC. Specimens were placed on the rack with the alphanumeric code on the underside (facing down and heretofore referred to as the back face). Whenever MMC or control specimens were recovered from the field, they were scanned or photographed in the uncleaned state. The disks used for bulk gravimetric corrosion measurements were then cleaned in a solution of phosphoric acid (H_3PO_4), chromium trioxide (CrO_3), and ultrapure (18.1 MΩ cm) water as described in ISO 8407 (*11*). The remaining disks were stored for further analyses and for characterizing the corrosion products.

For the cleaning operation, specimens were immersed in the just-described mildly heated phosphoric acid/chromium trioxide/water solution for 10 min at a temperature between 90 and 100 °C. They were then ultrasonically cleaned for 30 min in deionized water. After oven drying at 21 °C for 20–30 min, the specimens were reweighed on the same Mettler balance to determine weight loss. The initial and final weights were used, along with the surface area of each specimen to calculate the average weight loss per unit area for each MMC sample. The reported weight-loss data was the average value from two replicate samples; the data was reported as an average corrosion rate as grams per square meter per day (gmd). Figure 2 shows a macrograph of the front (upward facing, environmentally exposed) surface of a specimen before and after cleaning.

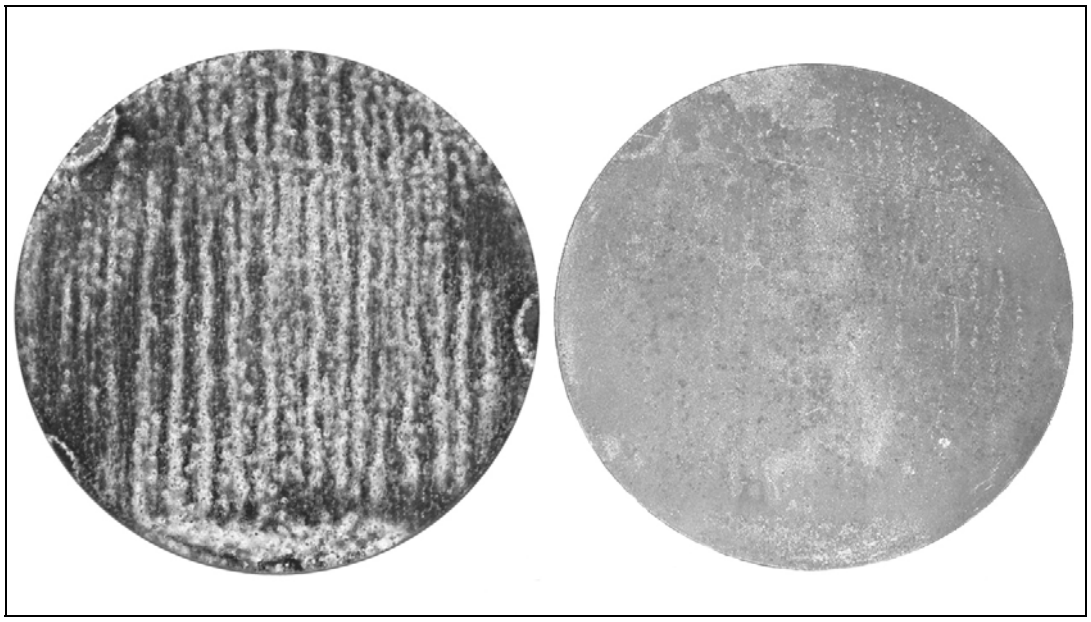

Figure 2. Before (left) and after (right) cleaning photos of 40 volume-percent SiC-reinforced Al MMC exposed for 90 days.

In addition to the MMCs at the Lyon test site, 10 6061 aluminum control specimens were also exposed for the same durations in order to obtain a nominal baseline corrosion weight loss per unit area of a monolithic alloy with a similar composition as the MMC matrix phase. The aluminum coupons, measuring 2 × 2 × 0.125 in, were stamped, cleaned, and weighed in the same manner as the eight reinforced MMC sample sets.

3.2 X-ray Diffraction (XRD) Characterization of Corrosion Products

XRD techniques were used as the major characterization procedure. The primary (metal matrix and ceramic reinforcement) phases were readily identifiable from prominent diffraction scan peak locations for each MMC and monolithic control sample. Comparing the differences between diffraction scans for the matched set of unexposed (virgin) samples with the exposed samples provided information about the nature of the corrosion product that overlies the original

substrate. Also, by measuring the decrement in the peak intensities of some major diffraction lines from the aluminum alloy substrate, calculations to determine the thickness of the oxide corrosion product layer were made. Similarly, the increase in the relative background count level of the exposed sample relative to the matched virgin sample provided another empirical measure of the overlying oxide thickness. Details about the Debye-Scherrer method to identify phases and the basic physics of x-ray absorption used to calculate the overlying oxide thickness can be found in Cullity (*12*). Specific details about calculating the thickness of an overlying surface layer of corrosion product from the peak intensity ratios of the exposed and virgin pair of samples will be presented subsequently.

A Philips Analytical powder diffraction system with a model PW1820 vertical goniometer and a copper target x-ray tube was used to collect diffraction scans from the Al MMC and monolithic aluminum control specimens. The goniometer was arranged with a 1° fixed divergence slit and a 0.2-mm receiving slit and operated in the step-scan mode with a 0.02° 2θ (diffraction angle) step size and a 2-s/step count time. The diffraction scans were acquired over a 2θ range of 20°–110° with the x-ray generator set at 45 kV and 40 mA. Philips X'Pert software was used for data collection and search-match analysis, with the candidate lines (peaks) compared against the International Centre for Diffraction Data (ICDD) Powder Diffraction File* for phase identification. Please note in figures 3–11 that the diffracted intensity is plotted as counts squared to emphasize the presence of low-intensity peaks. Also, the diffraction scans are displayed only for the 20°–70° 2θ range to enhance visualization of the x-ray peaks that were used for intensity-ratio calculations.

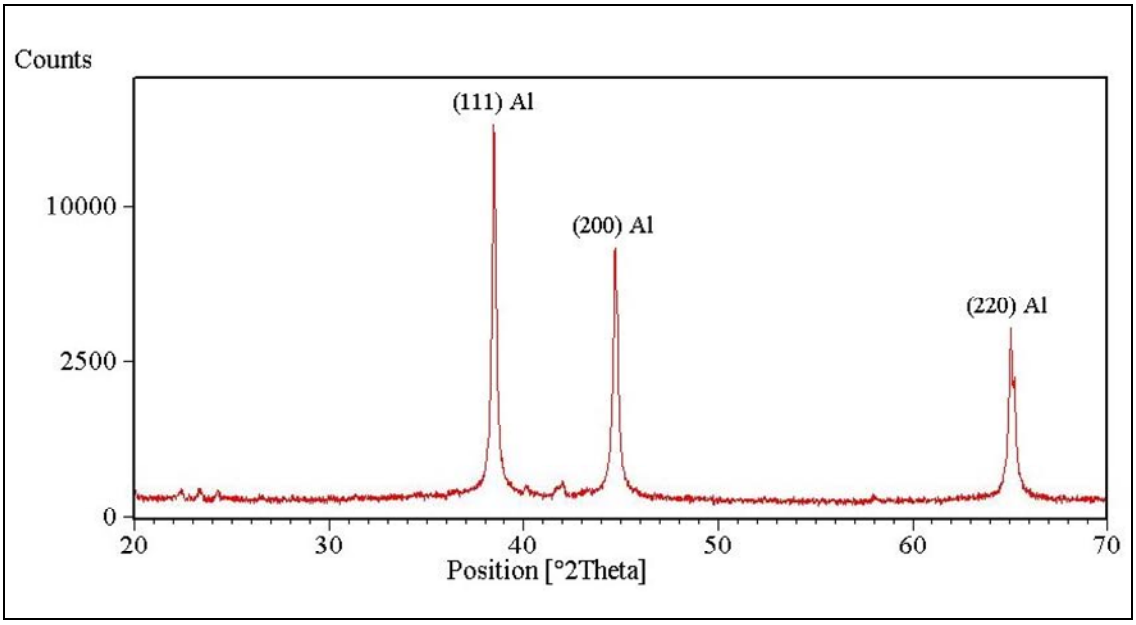

Figure 3. XRD scan of virgin monolithic aluminum.

* Powder Diffraction File is a trademark of JCPDS-International Center for Diffraction Data.

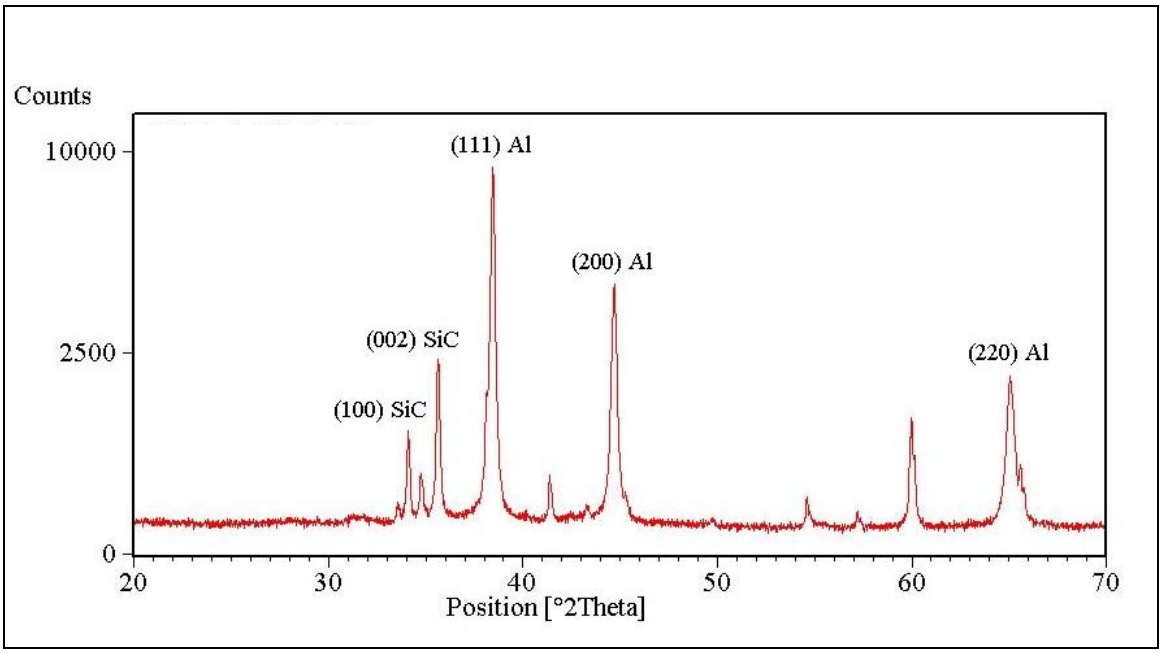

Figure 4. XRD scan of virgin 20-volume-percent black-SiC-reinforced Al MMC.

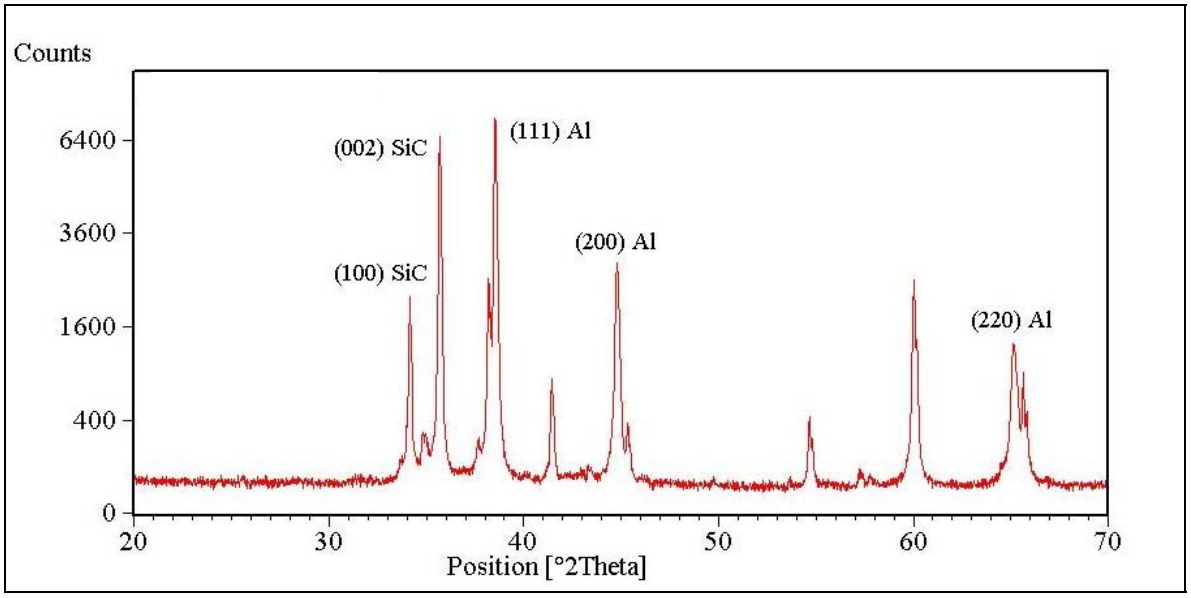

Figure 5. XRD scan of virgin 50-volume-percent black-SiC-reinforced Al MMC.

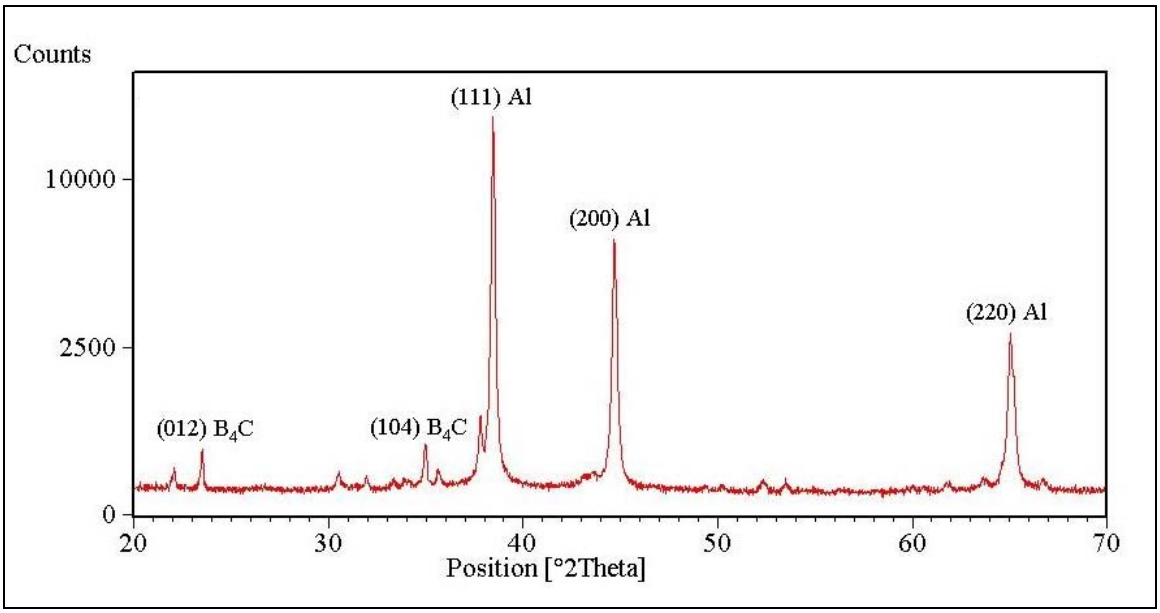

Figure 6. XRD scan of virgin 20-volume-percent B_4C-reinforced Al MMC.

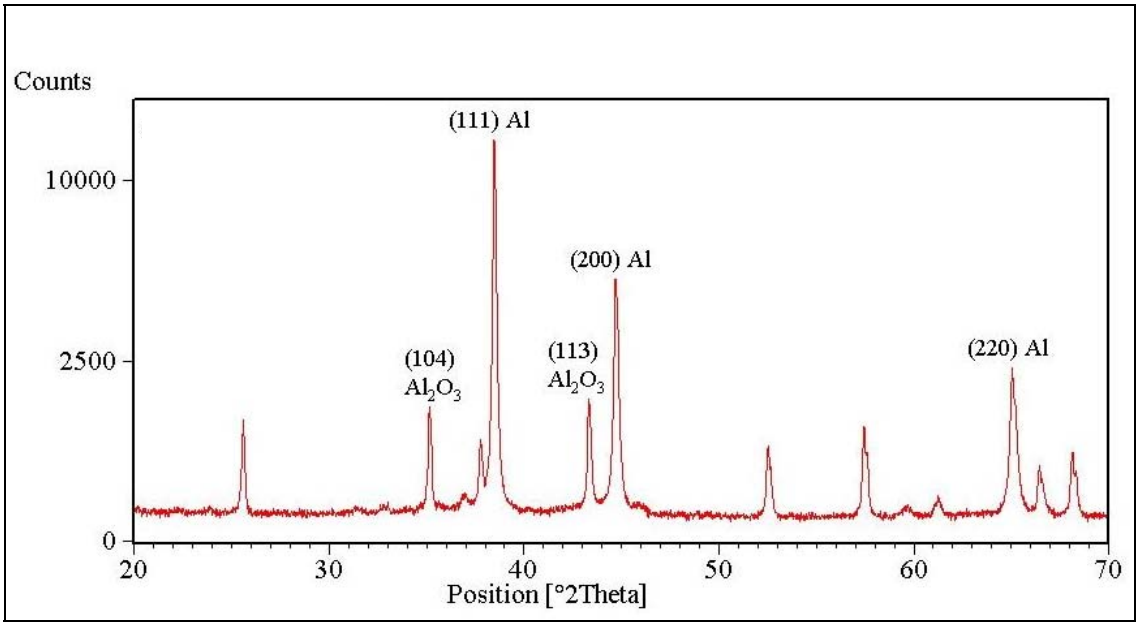

Figure 7. XRD scan of virgin 20-volume-percent Al_2O_3-reinforced Al MMC.

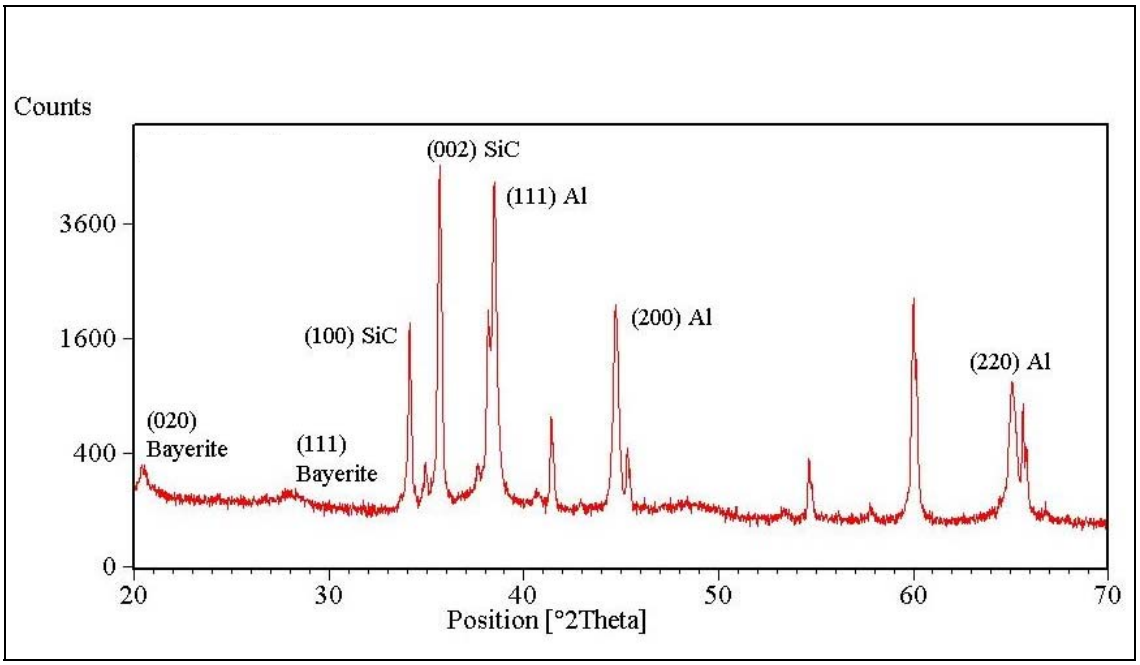

Figure 8. XRD scan of the front face of 50-volume-percent green-SiC-reinforced Al MMC after 12 months of outdoor exposure.

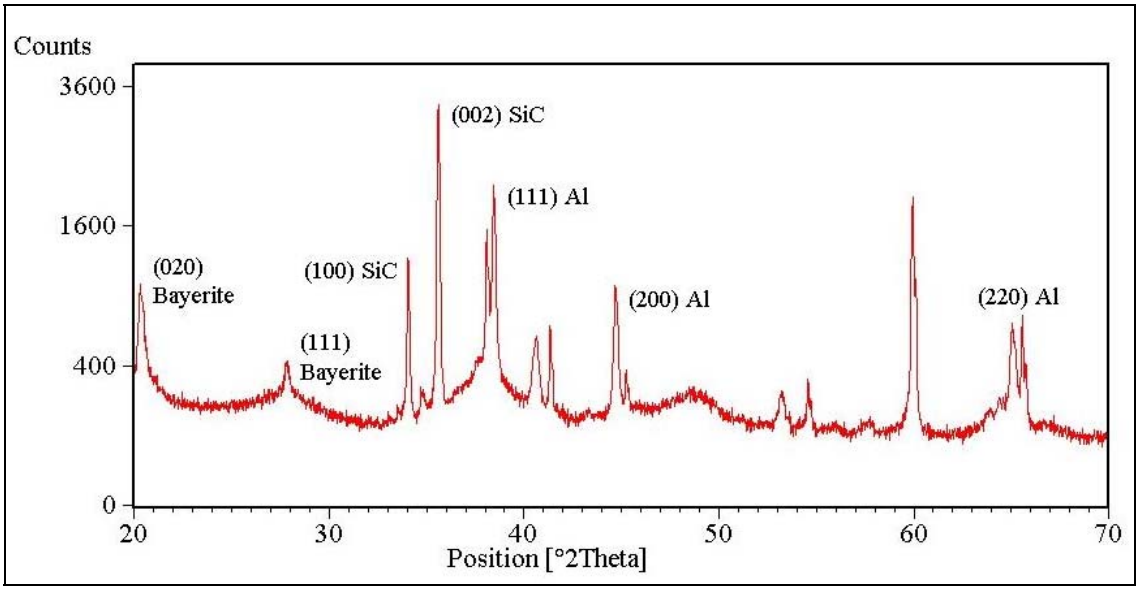

Figure 9. XRD scan of the front face of 50-volume-percent black-SiC-reinforced Al MMC after 12 months of outdoor exposure.

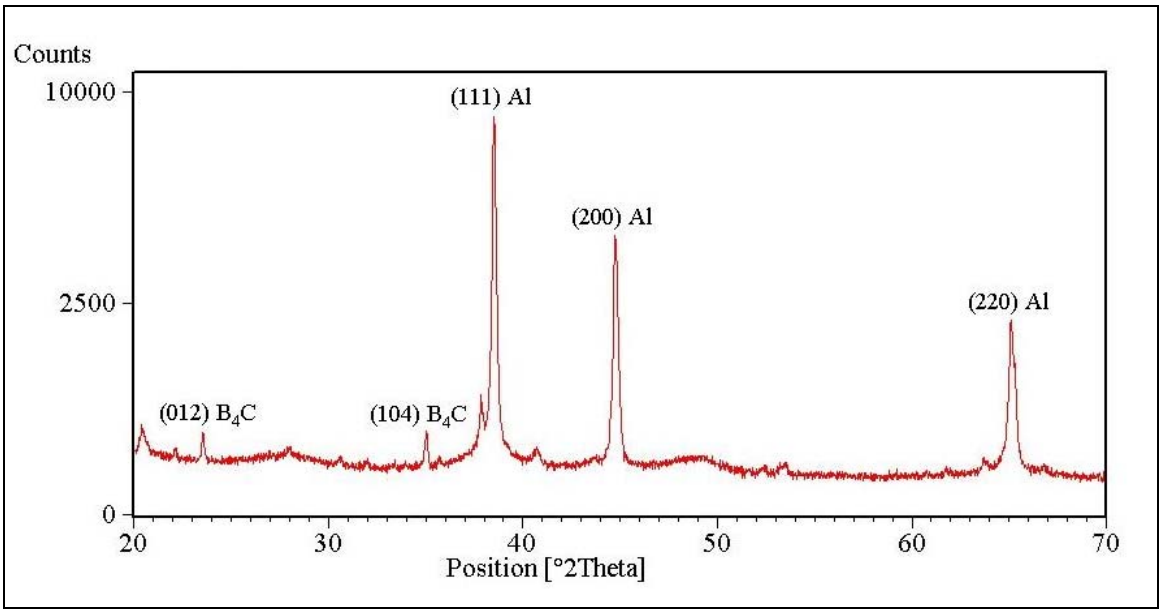

Figure 10. XRD scan of the front face of 20-volume-percent B_4C-reinforced Al MMC after 12 months of outdoor exposure.

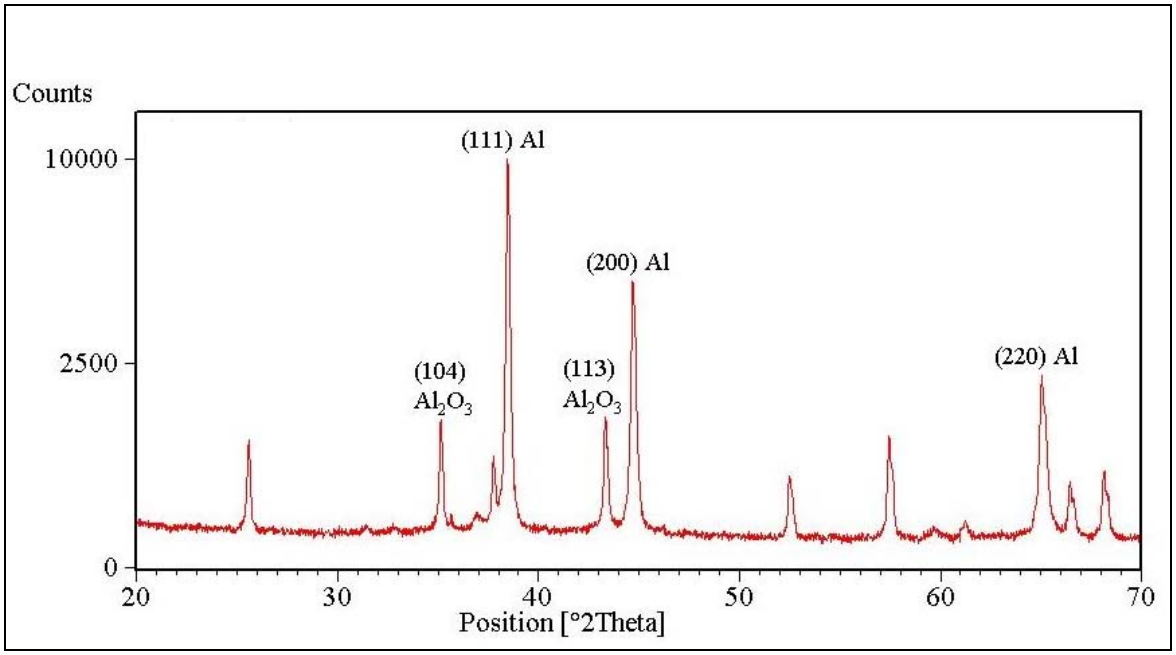

Figure 11. XRD scan of the front face of 20-volume-percent Al_2O_3-reinforced Al MMC after 12 months of outdoor exposure.

4. Experimental Results

4.1 Microstructural Observations

The microstructure of virgin samples is shown in figures 12–16. The various microstructures of these MMCs show the discontinuous arrangement of particles and the difference in particle sizes dependent on the volume-percent of the MMC.

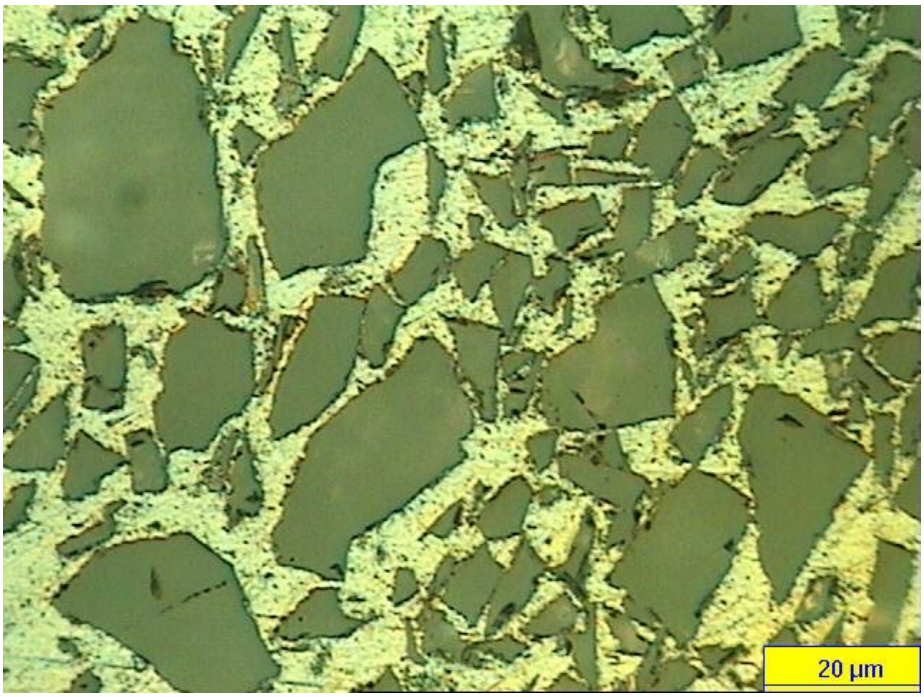

Figure 12. Microstructure of virgin 50-volume-percent green-SiC-reinforced Al MMC.

4.2 Gravimetric Observations

Tables 3 and 4 list the UH site gravimetric data for the 1-year weight-loss results from cleaned samples, as well as the weight gains for uncleaned characterization samples for the aluminum control samples, the 20- and 50-volume-percent black-SiC samples, the 50-volume-percent green-SiC sample, and the 20-volume-percent B_4C and Al_2O_3 samples.

4.3 XRD Characterization Studies

4.3.1 Diffraction Scans for Unexposed Substrate Phases

Typical diffraction scans for virgin samples of the control coupon (figure 3) and two different black-SiC (20 and 50 volume-percent) MMCs are shown in figures 4 and 5. The phase-analysis software identified the primary phases (Al and SiC) in the unexposed substrate. The Miller indices (hkl) and intensities of the corresponding prominent peaks from all the SiC-reinforced

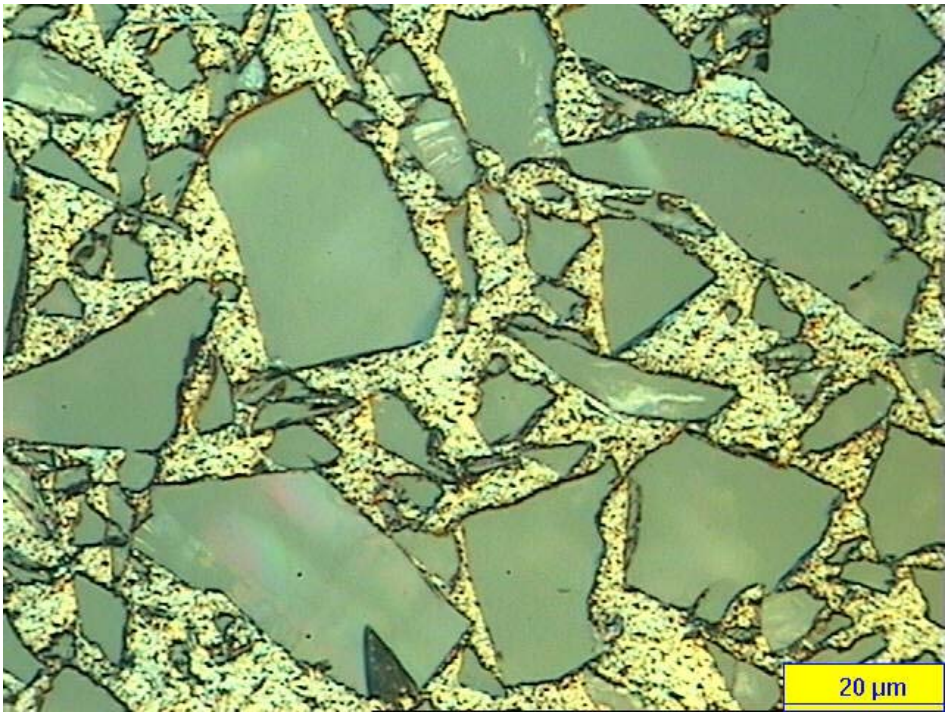

Figure 13. Microstructure of virgin 50-volume-percent black-SiC-reinforced Al MMC.

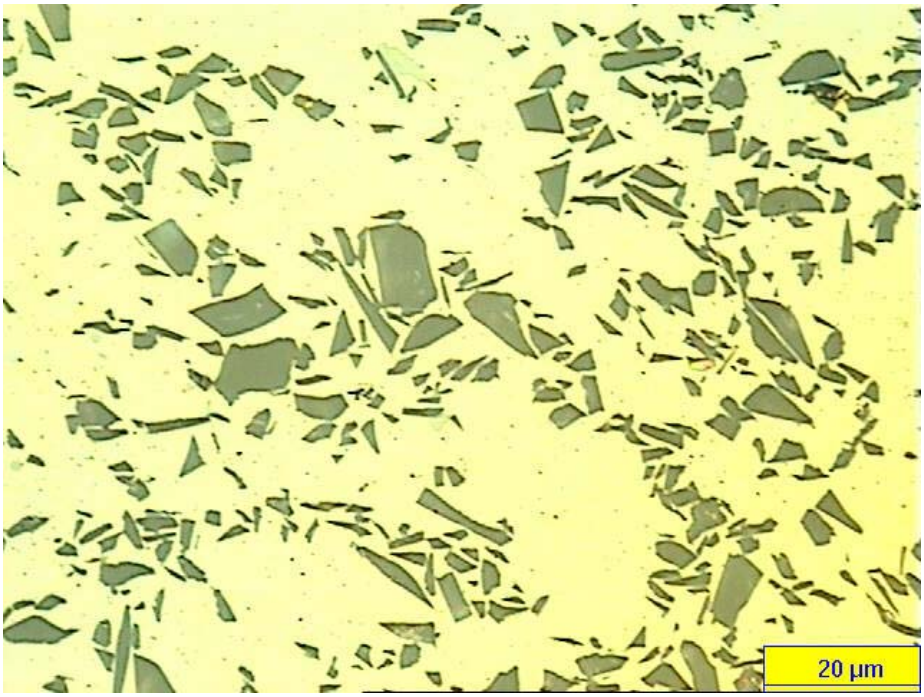

Figure 14. Microstructure of virgin 20-volume-percent black-SiC-reinforced Al MMC.

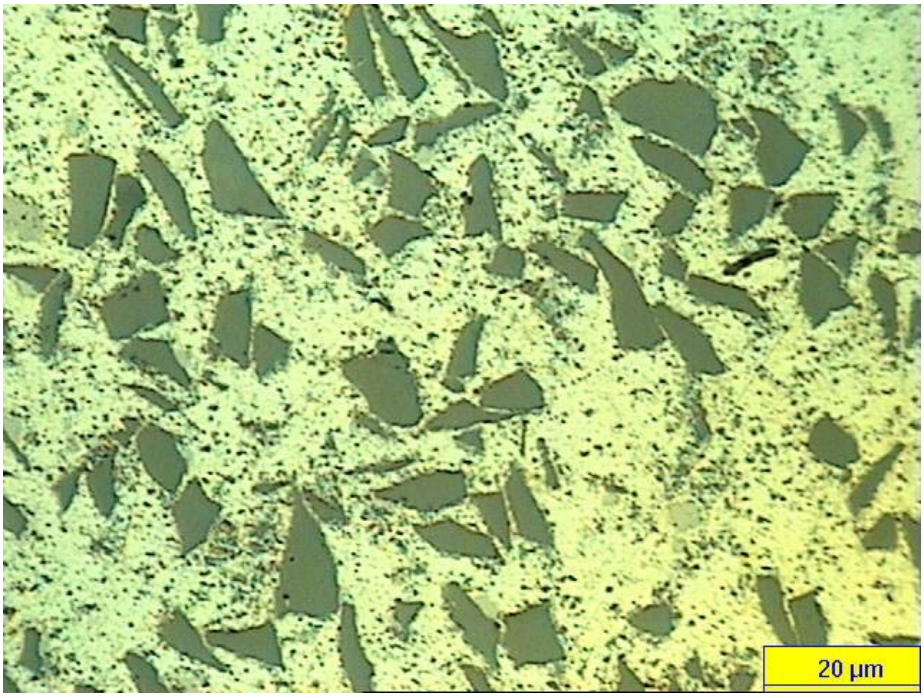

Figure 15. Microstructure of virgin 20-volume-percent B_4C-reinforced Al MMC.

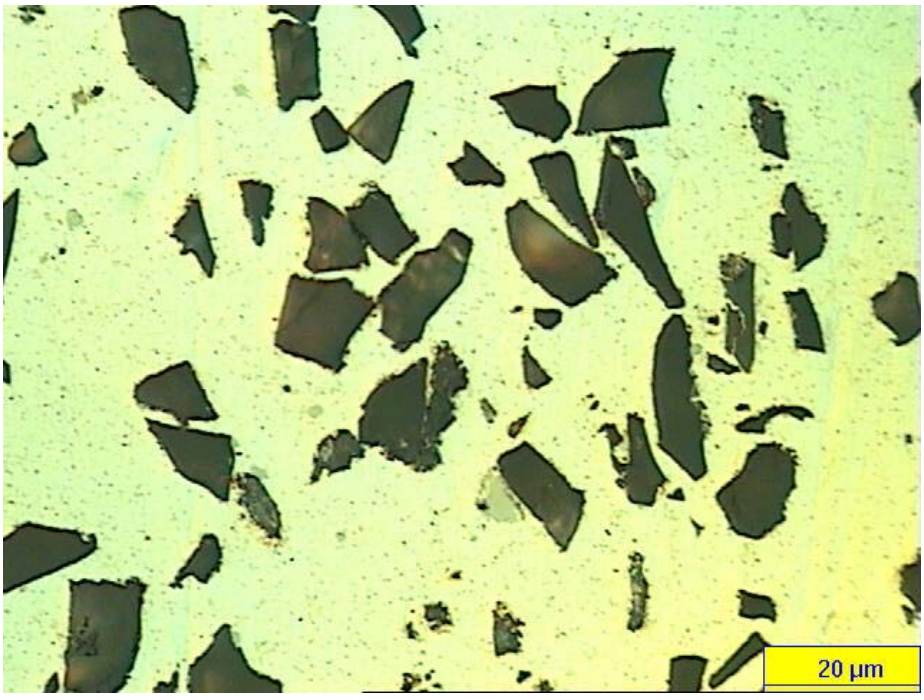

Figure 16. Microstructure of virgin 20-volume-percent Al_2O_3-reinforced Al MMC.

samples have been listed in table 5. Questionable or inconsistent data are marked with a question mark and ndl indicates that no diffraction line was present for that phase. Note that compared to the corresponding diffraction peaks from the monolithic control sample, the intensities from the aluminum-matrix peaks are reduced and, in general, are inversely proportional to the volume-percent of the SiC phase present in that MMC. The corresponding increase in all the SiC peak intensities is, again, generally proportional to the amount of SiC phase present in each MMC. Typical diffraction scans for virgin samples of the two other 20-volume-percent MMC variants with B_4C and $Al2O_3$ reinforcements are shown in figures 6 and 7. The phase-analysis software identified the primary phases in the unexposed substrate as aluminum and boron carbide or aluminum and corundum. The Miller indices and intensities of the corresponding prominent peaks for these MMCs have been listed in tables 6 and 7, respectively.

Table 3. Gravimetric measurements (cleaned specimens).

Specimen	Initial Weight (g)	Final Weight (g)	Change in Weight (g)	Average Change (g)	Corrosion Rate (gmd)
6061 Al (monolithic)	21.4056 21.4343	21.4039 21.4319	0.0017 0.0024	0.0021	0.00097261
6092 Al 20-volume-percent black SiC	47.7314 47.7186	47.6657 47.6562	0.0657 0.0624	0.0641	0.01234878
6092 Al 50-volume-percent black SiC	49.1076 49.1702	48.6768 48.8441	0.4308 0.3261	0.3785	0.07176491
6092 Al 50-volume-percent green SiC	48.5586	48.3209	0.2377	0.2377	0.04739349
6092 Al 20-volume-percent B_4C	44.8217 44.9342	44.4436 44.6625	0.3781 0.2717	0.3249	0.06161030
6092 Al 20-volume-percent Al_2O_3	47.9893 48.0114	47.8255 47.8330	0.1638 0.1784	0.1711	0.03469962

Table 4. Gravimetric measurements (uncleaned specimens).

Specimen	Initial Weight (g)	Final Weight (g)	Change in Weight (g)	Surface Area (cm^2)	Weight Change /Unit Area (g/cm^2)
6061 Al (monolithic)	21.4323	21.4368	0.0045	51.613	0.000087
6092 Al 20-volume-percent black SiC	47.7455	47.8077	0.0622	137.245	0.000453
6092 Al 50-volume-percent black SiC	49.2496	49.8476	0.5980	137.987	0.004333
6092 Al 50-volume-percent green SiC	47.3706	47.6614	0.2908	131.342	0.002214
6092 Al 20-volume-percent B_4C	44.7391	45.0951	0.3560	137.028	0.002598
6092 Al 20-volume-percent Al_2O_3	48.0078	48.1658	0.1580	130.080	0.001215

Table 5. XRD peak intensities for virgin and exposed 6061 aluminum and Al-SiC MMC specimens.

Specimen	Months Exposed	Face	Bayerite Phase		SiC Phase		Al Phase			Background Intensity at 23° 2θ
			(020) hkl, 20.3° 2θ	(111) hkl, 27.8° 2θ	(100) hkl, 34.1° 2θ	(002) hkl, 35.7° 2θ	(111) hkl, 38.5° 2θ	(200) hkl, 44.7° 2θ	(220) hkl, 65° 2θ	
6061 Al (monolithic)	0	Front	Ndl	Ndl	Ndl	Ndl	15751	7476	3668	38
		Back	—	—	—	—	—	—	—	—
	6	Front	Ndl	Ndl	Ndl	Ndl	13515	3439	7613 ?	40
		Back	Ndl	Ndl	Ndl	Ndl	15686	7161	4882 ?	38
	12	Front	Ndl	Ndl	Ndl	Ndl	14042	6166	5183 ?	37
		Back	Ndl	Ndl	Ndl	Ndl	11131	8001 ?	4729 ?	32
6092 Al 20-volume-percent black SiC	0	Front	Ndl	Ndl	888	2245	9228	4446	1873	62
		Back	Ndl	Ndl	873	2193	9170	5040	1850	62
	12	Front	Ndl	Ndl	847 ?	2340 ?	9790 ?	3106	1694	65
		Back	Ndl	Ndl	775	2410 ?	9983 ?	3440	1610	69
6092 Al 50-volume-percent black SiC	0	Front	Ndl	Ndl	2085	6354	7157	2687	1190	44
		Back	—	—	—	—	—	—	—	—
	6	Front	37	16	1838	5707	6028	2420	1102	110
		Back	95	50	2276 ?	6557 ?	5258	2106	935	102
	12	Front	772	192	1147	3069	1923	792	519	140
		Back	128	28	2088 ?	5627	5378	2003	1035	103
6092 Al 50-volume-percent green SiC	0	Front	Ndl	Ndl	2351	6674	6248	2800	1232	51
		Back	—	—	—	—	—	—	—	—
	12	Front	169	41	1756	4830	4422	1984	800	140
		Back	67	19	2689 ?	6538	5420	2400	1084	90

Notes: Ndl = no diffraction line was present.
? = questionable or inconsistent data.

Table 6. XRD peak intensities for virgin and exposed Al-B_4C MMC specimens.

Specimen	Months Exposed	Face	Bayerite Phase		B_4C Phase		Al Phase			Background Intensity at 23° 2θ
			(020) hkl, 20.3° 2θ	(111) hkl, 27.8° 2θ	(012) hkl, 23.5° 2θ	(104) hkl, 35° 2θ	(111) hkl, 38.5° 2θ	(200) hkl, 44.7° 2θ	(220) hkl, 65° 2θ	
6092 Al 20-volume percent B_4C	0	Front	Ndl	Ndl	326	378	13949	6408	2852	62
		Back	Ndl	Ndl	318	388	12990	6354	2547	60
	12	Front	293	74	175	234	8604	4048	2008	163
		Back	155	16	231	292	11080	5891	2311	69

Note: Ndl = no diffraction line was present.

Table 7. XRD peak intensities for virgin and exposed Al-Al_2O_3 MMC specimens.

Specimen	Months Exposed	Face	Bayerite Phase		Al_2O_3		Al Phase			Background Intensity at 23° 2θ
			(020) hkl, 20.3° 2θ	(111) hkl, 27.8° 2θ	(104) hkl, 35.1° 2θ	(113) hkl, 43.3° 2θ	(111) hkl, 38.5° 2θ	(200) hkl, 44.7° 2θ	(220) hkl, 65° 2θ	
6092 Al 20-volume-percent Al_2O_3	0	Front	Ndl	Ndl	1348	1414	12129	5144	2263	65
		Back	Ndl	Ndl	1336	1437	12108	5413	2310	70
	12	Front	17	Ndl	1194	1267	9788	4800	2164	92
		Back	206	27	973	1166	7539	3648	1782	142

Note: Ndl = no diffraction line was present.

4.3.2 Diffraction Scans for Exposed Samples With Substrate and Corrosion Product Phase

Typical diffraction scans from the front faces of the 12-month-exposed samples of the black and green SiC MMC variants are shown in figures 8 and 9, respectively. The phase-analysis software again identified the primary phases from the front and back faces of the exposed substrate as Al and SiC. Compared to the unexposed samples, the corresponding prominent peaks reappear but have attenuated intensities (see table 5). Typically, the attenuation of peak intensities from the back face is less than the front face. This observation can intuitively be interpreted (at least for the SiC-reinforced MMCs) that the corrosion film on the front face is thicker than that on the back face. Note the presence of two broad corrosion-product diffraction peaks labeled (020) Bayerite and (111) Bayerite that have been detected from the surfaces of the 50-volume-percent black and green SiC MMCs but are absent from the monolithic and 20-volume-percent SiC samples. Bayerite is a hydrated form of aluminum oxide with a density of ~3 g/cm^3. It is remarkable that these Bayerite peak intensities are greater on the sample front face than on the back face by a factor of 3. Consistent with gravimetric data and the aluminum peak-intensity attenuation observations, it is not surprising that the intensities of the 50-volume-percent black-SiC Bayerite peaks are substantially greater than the 50-volume-percent green-SiC Bayerite peaks on either of the corresponding front or back surfaces. One can speculate that the appearance of the crystalline (020) and (111) Bayerite peaks represent some form of amorphous-to-crystalline transformation of the original Bayerite corrosion film, especially as the surface layer grows in thickness.

Typical diffraction scans from the front faces of 12-month-exposed samples of two 20-volume-percent MMC variants with B_4C and Al_2O_3 reinforcements are shown in figures 10 and 11. The phase-analysis software again identified the primary phases as either aluminum and boron carbide or aluminum and corundum. The Miller indices and intensities of the corresponding prominent peaks for these MMCs from the front and back surfaces are listed in tables 6 and 7, respectively. Compared to the unexposed samples, the corresponding prominent peaks reappear but have attenuated intensities. For the boron-carbide MMC (and in common with the SiC MMC data), the attenuation of peak intensities from the back face being less than the front face and the presence of more intense Bayerite peaks diffracting from the front face should be noted. This combination of results leads to the interpretation that the corrosion film on the front face is much thicker than on the back face.

Counterintuitive results were detected for the alumina MMC. The attenuation of peak intensities from the front face being less than the back face, as well as the presence of more intense Bayerite peaks diffracting from the back face (see table 7), leads to the conflicting conclusion that the corrosion film on the back surface is thicker than on the front face, unlike the other sample results. Perhaps for the exposed alumina MMCs, solar irradiation might have impeded the corrosion process on the top surface; clearly, irradiation, climate, and humidity factors were

unchanged from the other (silicon-carbide- and boron-carbide-reinforced) MMC samples, since all of them were exposed for identical periods on the same rack.

4.3.3 Phase Identification of the Corrosion Film on Exposed Substrates

The original conceptual corrosion model for these environmentally exposed Al-MMC samples was that a semicontinuous film of corrosion product formed and chronologically grew in thickness over the substrate. The most likely oxidation product was some form of amorphous hydrated aluminum oxide since, in general, crystalline peaks of hydrated aluminum oxide were not detected by XRD on samples with environmental exposures of up to 6 months. In addition to the visually observed formation of a corrosion-product film on these samples, the XRD characterization results indicated that a substantial attenuation of the diffraction peaks from the primary aluminum and the crystalline reinforcement phase occurred and that there was a general increase of the overall low-angle background intensity values (arbitrarily measured at 23° 2θ), compared to the virgin counterpart samples, but it was not possible to determine the specific composition of this generic aluminum-oxide corrosion product. However, the increase in magnitude of this relative background intensity with exposure duration did track with the gravimetric data (see table 3), providing another indirect measure that the thickness of this amorphous corrosion layer was increasing with time. Fortunately, after 1 year, the detection of semicrystalline (020) and (111) Bayerite diffraction peaks for some MMC samples gave evidence that the originally formed amorphous phase was transforming into its crystalline state that was presumed to be of the same composition. Identifying Bayerite as the likely corrosion-film product will be used subsequently in corrosion-film-thickness calculations.

5. Discussion – Determining Corrosion Layer Thickness From X-ray Peak Attenuation Measurements

5.1 Derivation of Thickness Determining Formula

In order to quantify the effect of the overlying corrosion layer on attenuating diffracted beam intensities, an equation to determine such thicknesses (t) will be derived and adapted to the relevant diffractometer geometry. These calculations can be made by using the ratio of the diffracted peak (hkl) intensity of the virgin (v) sample $I_D(hkl)_v$ to that of an exposed (e) sample $I_D(hkl)_e$, along with handbook physical constants.

The first derivation is based on the generic linear attenuation absorption model (*12*). When x-rays with initial intensity I_o pass through a slab of absorbing material of thickness x, the resulting attenuation leads to a less-intense transmitted beam intensity I_x, as illustrated in figure 17. The relationship between the initial and the transmitted intensity is expressed in equation 1.

$$I_x = I_o \exp[-(u/r)rx]. \quad (1)$$

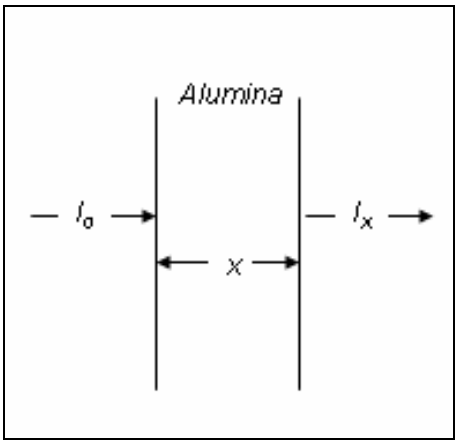

Figure 17. Linear x-ray-intensity absorption model.

The attenuation of the transmitted beam intensity, in addition to having a negative exponential relationship with the distance traversed in the absorbing layer, also is affected by the mass absorption coefficient (*u/r*) and the density (*r*) of that absorbing layer. Based on experimental insight for this x-ray characterization study that a corrosion layer formed on aluminum and Al-MMCs substrates, the value chosen for the alumina (or corundum) mass absorption coefficient was 26.71 cm^2/g and the density was nominally 3 g/cm^3 (for Bayerite alumina with three waters of hydration; note that a range of values exist that are a function of the number of waters of hydration). These constants should approximately match those for hydrated alumina and were used in calculating nominal film thicknesses (even if not exact, they certainly provided a ranking order of calculated thicknesses as a function of time and sample characteristics). Thus, even if other values are subsequently chosen, only some recalculation will be required to adjust the absolute values; this will certainly not affect the generally observed trends that provide significant insight for this study.

These absorption calculations need to be adapted for the appropriate diffractometer geometry (*12*) used to record diffracted peak intensities, as indicated in figure 18. Note the following linear and geometrical relationships:

- thickness of the continuous alumina film = t
- Bragg angle for (hkl) peak = 2θ
- total x-ray absorption path length in film = x = 2y = 2t/sinθ.

For the usual diffractometer geometry, the intensity diffracted by peak (hkl), $I_D(hkl)$, can be determined using equation 1 by inserting the total absorbing path length, x,

$$I_D(hkl) = I_o\exp[-(u/r)rx] = AI_o\exp[-(u/r)r2t/\sin\theta] , \qquad (2)$$

where A = diffraction intensity correction factor for each (hkl) peak.

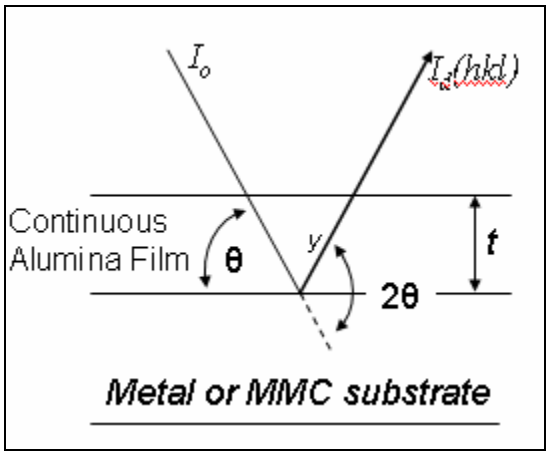

Figure 18. Corrosion film x-ray-intensity absorption model adapted to diffraction geometry.

For unexposed (virgin, v) samples where there is no corrosion overlayer (t = 0), equation 2 becomes

$$I_D(hkl)_v = A(hkl)I_o \quad . \tag{3}$$

After outdoor exposure (e), an oxide film of thickness t, forms, so that equation 2 now becomes

$$I_D(hkl)_e = A(hkl)I_o\exp[-(u/r)r\ 2t/\sin\theta]. \tag{4}$$

The corrosion product thickness t, is solved for from the ratio of equations 3 and 4,

$$t = ln[I_D(hkl)_v/I_D(hkl)_e]\sin\theta/[2(u/r)r]. \tag{5}$$

5.2 Calculated Corrosion-Product Thickness

Equation 5 was used to calculate the corrosion-product thicknesses for all the samples exposed for 1 year. The results for major diffraction peaks from the aluminum matrix and the respective reinforcement phases have been listed in tables 8–10.

Caveats for these measurements and calculations (that depend explicitly on the ratio of a series of single (hkl) peak intensity values but taken at different times) need to be outlined to explain a certain amount of variability/uncertainty apparent in these tables. First, it should be noted that the standard deviation for the accuracy of this data can be as high as 50%, especially when peak intensities are low, resulting in small, statistically undesirable peak-to-background ratios (*12*). This was the systematic case for certain weakly diffracting reinforcing phases, where only one or two major peak-intensity values were used for calculating thicknesses. Additionally, equipment-related factors can also produce small systematic or random drifts in incident radiation intensity, due to equipment and power supply variations; these in turn affect the exact magnitude of the measured diffracted peak intensities during an individual diffraction scan. Then there can be local variations in sample microstructure and corrosion rate variables (with kinetics that vary by

Table 8. Corrosion product thickness as a function of XRD peak intensity attenuations for virgin and exposed 6061 aluminum and Al-SiC MMC specimens.

Specimen	Months Exposed	Face	Peak Intensity		Thickness of Corrosion Product (µm)					Background Intensity at 23° 2θ
			Bayerite Phase		SiC Phase		Al Phase			
			(020) hkl, 20.3° 2θ	(111) hkl, 27.8° 2θ	(100) hkl, 34.1° 2θ	(002) hkl, 35.7° 2θ	(111) hkl, 38.5° 2θ	(200) hkl, 44.7° 2θ	(220) hkl, 65° 2θ	
6061 Al (monolithic)	0	Front	Ndl	Ndl	Ndl	Ndl	—	—	—	38
		Back	—	—	—	—	—	—	—	—
	12	Front	Ndl	Ndl	Ndl	Ndl	2.4	4.5	?	37
		Back	Ndl	Ndl	Ndl	Ndl	7.1	?	?	32
6092 Al 20-volume-percent black SiC	0	Front	Ndl	Ndl	—	—	—	—	—	62
		Back	Ndl	Ndl	—	—	—	—	—	62
	12	Front	Ndl	Ndl	?	?	?	10.2	3.2	65
		Back	Ndl	Ndl	?	?	?	7.8	4.8	69
6092 Al 50-volume-percent black SiC	0	Front	Ndl	Ndl	—	—	—	—	—	44
		Back	—	—	—	—	—	—	—	—
	12	Front	772	192	?	13.9	27	28.8	27.8	140
		Back	128	28	?	2.3	5.9	6.9	4.7	103
6092 Al 50-volume-percent green SiC	0	Front	Ndl	Ndl	—	—	—	—	—	51
		Back	—	—	—	—	—	—	—	—
	12	Front	169	41	?	6.2	7.1	8.1	14.5	140
		Back	67	19	?	0.39	2.9	2.8	4.3	90

Notes: Ndl = no diffraction line was present.
? = questionable or inconsistent data.

Table 9. Corrosion product thickness as a function of XRD peak intensity attenuations for virgin and exposed Al-B_4C MMC specimens.

Specimen	Months Exposed	Face	Peak Intensity		Thickness of Corrosion Product (µm)					Background Intensity at 23° 2θ
			Bayerite Phase		B_4C Phase		Al Phase			
			(020) hkl, 20.3° 2θ	(111) hkl, 27.8° 2θ	(012) hkl, 23.5° 2θ	(104) hkl, 35° 2θ	(111) hkl, 38.5° 2θ	(200) hkl, 44.7° 2θ	(220) hkl, 65° 2θ	
6092 Al 20-volume-percent B_4C	0	Front	Ndl	Ndl	—	—	—	—	—	62
		Back	Ndl	Ndl	—	—	—	—	—	60
	12	Front	293	74	7.8	9.2	9.2	10.7	9.9	163
		Back	155	16	4.2	5.1	4	1.9	5.2	69

Note: Ndl = no diffraction line was present.

Table 10. Corrosion product thickness as a function of XRD peak intensity attenuations for virgin and exposed Al-Al_2O_3 MMC specimens.

Specimen	Months Exposed	Face	Peak Intensity		Thickness of Corrosion Product (µm)					
			Bayerite Phase		Al_2O_3 Phase		Al Phase			Background Intensity at 23° 2θ
			(020) hkl, 20.3° 2θ	(111) hkl, 27.8° 2θ	(104) hkl, 35.1° 2θ	(113) hkl, 43.3° 2θ	(111) hkl, 38.5° 2θ	(200) hkl, 44.7° 2θ	(220) hkl, 65° 2θ	
6092 Al 20-volume-percent Al_2O_3	0	Front	Ndl	Ndl	—	—	—	—	—	65
		Back	Ndl	Ndl	—	—	—	—	—	70
	12	Front	17	Ndl	2.2	2.7	4.4	2.2	1.9	92
		Back	206	27	6.1	4.6	9.7	8.7	8.4	142

Note: Ndl = no diffraction line was present.

Table 11. Comparative values (from averaged diffraction peak results) of corrosion product thickness after 12 months of outdoor exposure.

Specimen	Weight Gain /Unit Area (g/cm^2)	Face	Nominal Value Over SiC Particles (µm)	Nominal Value Over B_4C Particles (µm)	Nominal Value Over Al_2O_3 Particles (µm)	Nominal Value Over Al Matrix (µm)
6061 Al (monolithic)	0.000087	Front	Ndl	Ndl	Ndl	3
		Back	Ndl	Ndl	Ndl	7 ?
6092 Al 20-volume-percent black SiC	0.000453	Front	?	Ndl	Ndl	9
		Back	?	Ndl	Ndl	7
6092 Al 50-volume-percent black SiC	0.004333	Front	13.9 ?	Ndl	Ndl	28
		Back	2.3	Ndl	Ndl	6
6092 Al 50-volume-percent green SiC	0.002214	Front	6.2	Ndl	Ndl	9
		Back	0.4 ?	Ndl	Ndl	3
6092 Al 20-volume-percent B_4C	0.002598	Front	Ndl	8.5	Ndl	10
		Back	Ndl	4.7	Ndl	3
6092 Al 20-volume-percent Al_2O_3	0.001215	Front	Ndl	Ndl	2.5	3
		Back	Ndl	Ndl	5.4	9

Notes: Ndl = no diffraction line was present.
? = questionable or inconsistent data.

a factor of 2 for samples in the same environment not being unusual) that further complicate the experimental data.

Despite these caveats, in general, the thickness values track consistently with the gravimetrically determined weight-change values as summarized in table 11, where averaged diffraction peak results from the aluminum matrix and the reinforcement phases after a 1-year exposure are presented. Except for the 20-volume-percent Al_2O_3 MMC with a thicker corrosion product layer on the back face, the reinforced Al-MMC samples had a thicker corrosion layer on the front, upward facing surface, with by far the thickest being the 28-μm layer present on the 50-volume-percent black SiC MMC, followed by three others in the 7–10-μm range. The corresponding back-face thicknesses ranged from 3 to 6 μm and were not consistent with the gravimetric trends. It was also interesting to note that the front-face corrosion-product thickness over the silicon-carbide particles was about 1/2 of that over the aluminum matrix, while the corrosion-product thicknesses over the reinforcing boron carbide and alumina particles were slightly less but similar to that over the aluminum matrix. (Further surface examination will be required to determine whether there is some continuity of the corrosion layer over the reinforcement particles or whether, if there is no local coverage, it is an artifact produced by the absorption of x-rays passing at a diffraction angle θ through the corrosion product growing above the adjacent aluminum-matrix phase). For the 20-volume-percent reinforcement phase series, the boron-carbide MMC had a thicker front-face corrosion layer than the silicon-carbide MMC (both based on gravimetric and film-thickness results). The alumina-reinforced MMC with the intermediate gravimetric result and the contrary presence of a thinner front face and a thicker back-face corrosion layer will clearly need to be investigated further.

6. Conclusions

6.1 Outdoor-Exposure Corrosion Rates

Although this report covers observations from only a limited set of monolithic and Al-MMC samples subjected to 1 year of atmospheric exposure at a single (but climatologically the wettest) HCL location, some trends are clearly visible from the gravimetric corrosion data. For comparable exposure times, all of these MMCs have a corrosion rate that is at least an order of magnitude greater than a similar monolithic aluminum alloy. The bulk corrosion rate of MMCs reinforced with black SiC generally increases with an increase in volume fraction of the reinforcement. This increase in corrosion rate appears to be (more than linearly) proportional to the volume fraction of the SiC (where the gravimetric rate for 50-volume-percent SiC MMC is at least 5× greater than the 20-volume-percent SiC MMC even though the 50-volume-percent SiC sample presented 1/3 less aluminum-matrix-phase surface area to react). Also, the corrosion rate for the 50-volume-percent black-SiC MMC was about twice that of the 50-volume-percent green-SiC MMC that is of higher purity and higher resistivity. This would be expected because of galvanic action if the black SiC supports cathodic currents. However, the 50-volume-percent

green SiC had a higher corrosion rate than the 20-volume-percent black-SiC MMC, indicating that reinforcement phase content was also significant.

Of the three 20-volume-percent MMCs with different reinforcement species, the B_4C MMC generally corroded at a higher rate than those reinforced with either Al_2O_3 (with an intermediate rate) or SiC (with the lowest rate). Also, the 20-volume-percent B_4C MMC with significantly less reinforcement phase had a higher corrosion rate than the 50-volume-percent green SiC. This trend is also likely due in part to the resistivity of the reinforcements, since B_4C generally has low resistivity, SiC has wide fluctuations in resistivity depending on purity, and Al_2O_3 is an insulator. Although there is a trend for the corrosion rate to increase with increased reinforcement content, there is now strong evidence that the type of reinforcing phase can strongly influence the atmospheric corrosion rate of that MMC. Thus, those MMCs with higher resistivity reinforcement particles tend to have comparably lower corrosion rates.

These outdoor-exposure tests generally support the hypothesis that corrosion is related to the conductivity and the volume fraction of the reinforcement specie. Corrosion rates increased as the content of black SiC was increased. For the same volume fractions, the corrosion rates were lower in MMCs reinforced with high-purity green SiC than for those with black SiC. Corrosion rates were higher for MMCs reinforced with B_4C than they were for MMCs reinforced with equal amounts of either SiC or Al_2O_3.

6.2 Characterizing the Corrosion-Product Layers

Experimental XRD data for virgin and exposed samples of the control coupon and the five MMC variants yielded quantitative and qualitative characterization of the atmospheric corrosion products that formed on these samples during their 1-year outdoor exposure. Further analysis using intensity ratios of the virgin and exposed samples provided semiquantitative measures of the corrosion-product thickness.

For the exposed samples, the relative intensities of the aluminum and the reinforcement diffraction peaks decrease significantly relative to those from their comparable virgin samples. The attenuation of the peak-intensity values was found to be somewhat proportional to the thickness of corrosion product that formed over the original substrate. Typically, for all but the exposed 20-volume-percent alumina MMC sample, the observed attenuation of the peak-intensity values was greater for XRD scans obtained from the front (upward facing) surfaces than from the back surfaces of each sample, indicating that the front surface had a thicker corrosion product. By far, the largest corrosion-layer thickness (28 μm) was calculated for the front surface of the 50-volume-percent black-SiC MMC, and this was consistent with the gravimetric data—three of the other four reinforced MMCs were in the 9–10-μm range. Nearly all of the back surfaces had 3–6-μm thicknesses, with the exception of the anomalous 20-volume-percent alumina MMC sample with 3- and 9-μm front and back thicknesses, respectively.

For the XRD scans from the monolithic control and the 20-volume-percent black-SiC MMC samples exposed for 1-year, peak-intensity attenuations resulted in peaks that were nominally 80% of those from virgin samples, with no evidence of a crystalline-hydrated aluminum oxide-phase. Thus, it was concluded that the overlying corrosion product that caused the observed peak-intensity attenuations was due to the presence of a semicontinuous hydrated aluminum oxide layer that also increased the low-angle background intensities. But since no crystalline-hydrated aluminum-oxide diffraction peaks were detected, the attenuation was attributed to an overlying amorphous Bayerite corrosion-product layer.

Most of the rest of the exposed samples' XRD scans had greater peak-intensity attenuations consistent with the presence of thicker corrosion-product layers. In addition, all of these XRD scans (including the anomalous 20-volume-percent alumina MMC sample) had two other distinct general features that were metrified (see tables 8–10): the background levels of XRD scans were elevated (the arbitrary values reported were for the background intensity at $2\theta = 23^{o}$, chosen because no overlapping crystalline peaks appeared in any XRD scan), and the presence of semicrystalline alumina namely, (020) Bayerite and (111) Bayerite diffraction peaks that appeared as a crystalline peaks (with measurable peak intensities that proved to be a good metric) emerging from an amorphous hump. These metrics qualitatively tracked well with and were inversely proportional to the attenuation of the substrate phase(s) diffraction peak intensities, thus, indirectly substantiating the corrosion-product-thickness calculation results.

7. Summary

In general, this corrosion-product characterization study provided important insights into procedures for measuring Al MMC corrosion. It is intuitively obvious that corrosion phenomena and kinetics on the front and back faces of outdoor-corrosion specimens should be different, and this study has quantified these differences. In most cases, the thickness of the corrosion-product layer on the front surface exceeds that on the back surface since environmental effects such as solar irradiation and/or the extended presence of water/electrolyte films should be greater on the upward facing sample face. However, the caveat is that bulk gravimetric measurements of corrosion (rates) only represent the weighted average of the phenomena occurring on the upward facing and back surfaces. Thus, care in interpreting any gravimetric corrosion measurement results is recommended.

The case for the anomalous reversal of thicknesses on front and back surfaces of the 20-volume-percent alumina MMC sample deserves further study to confirm whether the results are repeatable. If this phenomenon is real, fundamental studies should be undertaken to discover what physical phenomena in the reinforcement phase can impede and/or accelerate corrosion kinetics. One can speculate that for this specific MMC, the presence or absence of solar irradiation may affect the properties of certain forms of crystalline Al_2O_3 that, in turn, may alter the kinetics and/or mechanism of Al-MMC corrosion.

For applications that consider utilizing Al-MMCs components for their superior mechanical properties, appropriate regard should be taken for the lowered environmental durability of these materials relative to monolithic aluminum alloys. This limitation can be compensated for by designing in greater thicknesses for that component or by using suitable corrosion-mitigating coatings or other surface treatments.

8. References

1. Ceradyne, Inc. Home Page. http://www.ceradyne.com (accessed April 2002).
2. Ichinose, N. *Introduction to Fine Ceramics*; Wiley: New York, NY, 1987; pp 50–52.
3. Bolz, R. E.; Tuve, G. L. *CRC Handbook of Tables for Applied Engineering Science, 2nd Ed.*; CRC Press: Boca Raton, FL, 1973; pp 262–264.
4. Goodfellow Corp. *Metals and Materials Catalog*; Oakdale, PA, 1991–1992.
5. DWA Aluminum Composites Home Page. http://www.dwa-dra.com (accessed May 2003).
6. Goodfellow Corp. Technical Data Sheet. http://www.goodfellow.com (accessed May 2003).
7. Hihara, L. H. Corrosion of Metal Matrix Composites. *Corrosion: Materials, Environments, and Industries*; American Society of Metals International: Materials Park, OH, 2005.
8. Hihara, L. H. Metal-Matrix Composites. In *Manual on Corrosion Tests and Standards: Application and Interpretation, 2nd Ed.*; American Society for Testing and Materials International: West Conshohocken, PA, 2005.
9. Wylie, R. G. *Humidity and Moisture*. Wexler, A., Ed.; Reinhold Publishing Corp.: New York, NY, 1964; p 507.
10. Hongbo, D.; Hihara, L. H. Localized Corrosion Currents and pH Profile over B_4C, SiC, and Al_2O_3 Reinforced 6092 Aluminum Composites in 0.5M Na_2SO_4 Solution. *Journal of the Electrochemical Society* **2005**, *152*, (4).
11. ISO 8407. *Corrosion of Metals and Alloys – Removal of Corrosion Products from Corrosion Test Specimens* **1991**.
12. Cullity, B. D. *Elements of X-Ray Diffraction, 2nd Ed.*; Addison-Wesley: Reading, MA, 1978.

NO. OF
COPIES ORGANIZATION

1 (PDF ONLY) DEFENSE TECHNICAL INFORMATION CTR
DTIC OCA
8725 JOHN J KINGMAN RD
STE 0944
FORT BELVOIR VA 22060-6218

1 US ARMY RSRCH DEV & ENGRG CMD
SYSTEMS OF SYSTEMS INTEGRATION
AMSRD SS T
6000 6TH ST STE 100
FORT BELVOIR VA 22060-5608

1 DIRECTOR
US ARMY RESEARCH LAB
IMNE ALC IMS
2800 POWDER MILL RD
ADELPHI MD 20783-1197

1 DIRECTOR
US ARMY RESEARCH LAB
AMSRD ARL CI OK TL
2800 POWDER MILL RD
ADELPHI MD 20783-1197

ABERDEEN PROVING GROUND

1 DIR USARL
AMSRD ARL CI OK TP (BLDG 4600)

NO. OF COPIES ORGANIZATION

1 DIRECTOR
US ARMY RSRCH LAB
AMSRD ARL SE DE
R ATKINSON
2800 POWDER MILL RD
ADELPHI MD 20783-1197

2 DIRECTOR
US ARMY RSRCH LAB
AMSRD ARL WM MB
M BERMAN
M CHOWDHURY
2800 POWDER MILL RD
ADELPHI MD 20783-1197

1 COMMANDER
US ARMY MATERIEL CMD
AMXMI INT
9301 CHAPEK RD
FORT BELVOIR VA 22060-5527

2 PM MAS
SFAE AMO MAS MC
PICATINNY ARSENAL NJ
07806-5000

1 US ARMY ARDEC
AMSRD AAR AEM D
J LUTZ
BLDG 354
PICATINNY ARSENAL NJ
07806-5000

1 DEPT OF THE ARMY
RDECOM ARDEC
AMSRD AAR EMO F
BLDG 1
PICATINNY ARSENAL NJ
07806-5000

1 US ARMY ARDEC
AMSRD AAR AEM
M PALATHINGAL
BLDG 65 SOUTH
PICATINNY ARSENAL NJ
07806-5000

NO. OF COPIES ORGANIZATION

1 US ARMY ARDEC
AMSTA AR CCH A
F ALTAMURA
BLDG 354
PICATINNY ARSENAL NJ
07806-5000

1 US ARMY ARDEC
AMSTA AR CCH A
R HOWELL
BLDG 65 NORTH
PICATINNY ARSENAL NJ
07806-5000

1 US ARMY ARDEC
AMSTA AR CCH A
L MANOLE
BLDG 65 SOUTH
PICATINNY ARSENAL NJ
07806-5000

1 US ARMY ARDEC
AMSRD AAR AEM L
A VELLA
BLDG 354
PICATINNY ARSENAL NJ
07806-5000

1 US ARMY ARDEC
AMSRD AAR AEM L
D VO
BLDG 65 SOUTH
PICATINNY ARSENAL NJ
07806-5000

1 US ARMY ARDEC
AMSRD AAR AEM T
M NICOLICH
BLDG 65 SOUTH
PICATINNY ARSENAL NJ
07806-5000

1 US ARMY ARDEC
AMSRD AAR AEM
M LUCIANO
BLDG 65 SOUTH
PICATINNY ARSENAL NJ
07806-5000

NO. OF COPIES ORGANIZATION

1 US ARMY ARDEC
AMSRD AAR AEM
S MUSALLI
BLDG 65 SOUTH
PICATINNY ARSENAL NJ
07806-5000

1 US ARMY ARDEC
AMSRD AAR EBM
R CARR
BLDG 1
PICATINNY ARSENAL NJ
07806-5000

1 US ARMY ARDEC
SFAE AMO MAS SETI
T C LIVECCHIA
BLDG 354 SOUTH
PICATINNY ARSENAL NJ
07806-5000

1 US ARMY ARDEC
AMSRD AAR AEM L
M YOUNG
BLDG 65 SOUTH
PICATINNY ARSENAL NJ
07806-5000

1 US ARMY ARDEC
AMSRD AAR AEM C
D DEMELLA
BLDG 61 SOUTH
PICATINNY ARSENAL NJ
07806-5000

1 US ARMY ARDEC
AMSRD AAR AEM
S CHICO
BLDG 65 SOUTH
PICATINNY ARSENAL NJ
07806-5000

1 US ARMY ARDEC
SFAE AMO MAS LC
D RIGOGLIOSO
BLDG 354 M829E3 IPT
PICATINNY ARSENAL NJ
07806-5000

NO. OF COPIES ORGANIZATION

1 US ARMY ARDEC
AMSRD AAR AEM L
P DONADIA
BLDG 65 SOUTH
PICATINNY ARSENAL NJ
07806-5000

1 US ARMY ARDEC
AMSTA AR CCH B
K HENRY
BLDG 95
PICATINNY ARSENAL NJ
07806-5000

1 US ARMY ARDEC
AMSRD AAR AEM L
F DONLON
BLDG 65 SOUTH
PICATINNY ARSENAL NJ
07806-5000

1 PM MAS
SFAE AMO MAS
PICATINNY ARSENAL NJ
07806-5000

1 US ARMY ARDEC
SFAE AMO MAS LC
P VALENTI
BLDG 354
PICATINNY ARSENAL NJ
07806-5000

1 US ARMY ARDEC
AMSRD AAR AEM L
R SAYER
BLDG 65
PICATINNY ARSENAL NJ
07806-5000

1 US ARMY ARDEC
SFAE AMO MAS LC
F CHANG
BLDG 354
PICATINNY ARSENAL NJ
07806-5000

NO. OF COPIES ORGANIZATION

1 PM ARMS
AMSRD AAR EMB
J BRESCIA
BLDG 1
PICATINNY ARSENAL NJ
07806-5000

1 PM MAS
SFAE AMO MAS
CHIEF ENGINEER
PICATINNY ARSENAL NJ
07806-5000

1 PM MAS
SFAE AMO MAS PS
PICATINNY ARSENAL NJ
07806-5000

2 PM MAS
SFAE AMO MAS LC
PICATINNY ARSENAL NJ
07806-5000

1 COMMANDER
US ARMY TACOM
AMSTA SF
WARREN MI 48397-5000

1 COMMANDER
US ARMY TACOM
PM COMBAT SYSTEMS
SFAE GCS CS
6501 ELEVEN MILE RD
WARREN MI 48397-5000

2 OFC OF NAVAL RSRCH
J CHRISTODOULOU
D SHIFLER
ONR CODE 332
800 N QUINCY ST
ARLINGTON VA 22217-5600

1 COMMANDER
US ARMY TACOM
PM SURVIVABLE SYSTEMS
SFAE GCSS W GSI H
M RYZYI
6501 ELEVEN MILE RD
WARREN MI 48397-5000

NO. OF COPIES ORGANIZATION

1 COMMANDER
US ARMY TACOM
CHIEF ABRAMS TESTING
SFAE GCSS W AB QT
J MORAN
6501 ELEVEN MILE RD
WARREN MI 48397-5000

1 COMMANDER
WATERVLIET ARSENAL
SMCWV QAE Q
B VANINA
BLDG 44
WATERVLIET NY 12189-4050

2 SFSJM CDL
HQ US ARMY JNT MUNITIONS CMND
AMSIO SMT
R CRAWFORD
W HARRIS
1 ROCK ISLAND ARSENAL
ROCK ISLAND IL 61299-6000

2 COMMANDER
US ARMY AMCOM
AVIATION APPLIED TECH DIR
J SCHUCK
FORT EUSTIS VA 23604-5577

1 NSWC
DAHLGREN DIV CODE G06
DAHLGREN VA 22448

2 US ARMY CORPS OF ENGR
CERD C
T LIU
CEW ET
T TAN
20 MASSACHUSETTS AVE NW
WASHINGTON DC 20314

1 US ARMY TARDEC
AMSRD TAR R
D TEMPLETON
6501 E 11 MILE RD MS 263
WARREN MI 48397-5000

NO. OF COPIES	ORGANIZATION
3	USA SBCCOM MATERIAL SCIENCE TEAM AMSSB RSS J HERBERT M SENNETT L-A BARKHOUSE KANSAS ST NATICK MA 01760-5057
2	COMMANDER US ARMY RDECOM AMSTA TR R J BENNETT D HANSEN MS 271 WARREN MI 48397-5000
1	COMMANDER US ARMY RDECOM AMSTA TR D D OSTBERG MS 263 WARREN MI 48397-5000
1	USA SBCCOM PM SOLDIER SPT AMSSB PM RSS A J CONNORS KANSAS ST NATICK MA 01760-5057
7	BENET LABS AMSTA AR CCB R FISCELLA G SPENCER R HASENBEIN AMSTA CCB R S SOPOK E HYLAND D CRAYON R DILLON WATERVLIET NY 12189-4050
1	NSWC TECH LIBRARY CODE B60 17320 DAHLGREN RD DAHLGREN VA 22448
1	NSWC CRANE DIV M JOHNSON CODE 20H4 LOUISVILLE KY 40214-5245
2	NSWC U SORATHIA C WILLIAMS CODE 6551 9500 MACARTHUR BLVD WEST BETHESDA MD 20817
2	COMMANDER NSWC CARDEROCK DIV R PETERSON CODE 2020 M CRITCHFIELD CODE 1730 BETHESDA MD 20084
1	NAVAL SEA SYSTEMS CMND D LIESE 1333 ISAAC HULL AVE SE 1100 WASHINGTON DC 20376-1100
7	DIRECTOR US ARMY NGIC D LEITER MS 404 M HOLTUS MS 301 M WOLFE MS 307 S MINGLEDORF MS 504 J GASTON MS 301 W GSTATTENBAUER MS 304 J CRIDER MS 306 2055 BOULDERS RD CHARLOTTESVILLE VA 22911-8318
1	AFRL MLBC 2941 P ST RM 136 WRIGHT PATTERSON AFB OH 45433-7750
1	DIRECTOR LOS ALAMOS NATL LAB F L ADDESSIO T 3 MS 5000 PO BOX 1633 LOS ALAMOS NM 87545
1	NSWC CARDEROCK DIV R CRANE CODE 6553 9500 MACARTHUR BLVD WEST BETHESDA MD 20817-5700
1	AFRL MLMP R THOMSON 2977 HOBSON WAY BLDG 653 RM 215 WRIGHT PATTERSON AFB OH 45433-7739

NO. OF COPIES	ORGANIZATION
6	US ARMY RSRCH OFC H EVERITT J PRATER G ANDERSON D STEPP D KISEROW D SKATRUD PO BOX 12211 RESEARCH TRIANGLE PARK NC 27709-2211
7	US ARMY SBCCOM SOLDIER SYSTEMS CTR BALLISTICS TEAM J WARD W ZUKAS P CUNNIFF J SONG MARINE CORPS TEAM J MACKIEWICZ AMSSB RCP SS W NYKVIST S BEAUDOIN KANSAS ST NATICK MA 01760-5019
8	NSWC J FRANCIS CODE G30 D WILSON CODE G32 R D COOPER CODE G32 J FRAYSSE CODE G33 E ROWE CODE G33 T DURAN CODE G33 L DE SIMONE CODE G33 R HUBBARD CODE G33 DAHLGREN VA 22448
2	AFRL MLMP F ABRAMS J BROWN 2977 HOBSON WAY BLDG 653 RM 215 WRIGHT PATTERSON AFB OH 45433-7739
1	DIRECTOR LLNL STEVE DETERESA PO BOX 808 LIVERMORE CA 94550

NO. OF COPIES	ORGANIZATION
1	DIRECTOR LLNL L-125 FRANK MAGNESS PO BOX 808 LIVERMORE CA 94550
1	DIRECTOR LLNL L-020 MILTON FINGER PO BOX 808 LIVERMORE CA 94550
1	DIRECTOR LLNL L-099 MIKE MURPHY PO BOX 808 LIVERMORE CA 94550
1	AFRL MLS OL L COULTER 5851 F AVE BLDG 849 RM AD1A HILL AFB UT 84056-5713
1	OSD JOINT CCD TEST FORCE OSD JCCD R WILLIAMS 3909 HALLS FERRY RD VICKSBURG MS 29180-6199
2	DARPA S WAX L CHRISTODOULOU 3701 N FAIRFAX DR ARLINGTON VA 22203-1714
1	OAK RIDGE NATL LAB R M DAVIS PO BOX 2008 OAK RIDGE TN 37831-6195
1	OAK RIDGE NATL LAB C EBERLE MS 8048 PO BOX 2008 OAK RIDGE TN 37831
3	NIST J CHIN MS 8621 J MARTIN MS 8621 D DUTHINH MS 8611 100 BUREAU DR GAITHERSBURG MD 20899

NO. OF COPIES ORGANIZATION

1 OAK RIDGE NATL LAB
C D WARREN MS 8039
PO BOX 2008
OAK RIDGE TN 37831

1 HYDROGEOLOGIC INC
SERDP ESTCP SPT OFC
S WALSH
1155 HERNDON PKWY STE 900
HERNDON VA 20170

3 DIRECTOR
SANDIA NATL LABS
APPLIED MECHS DEPT
MS 9042
J HANDROCK
Y R KAN
J LAUFFER
PO BOX 969
LIVERMORE CA 94551-0969

2 NASA LANGLEY RSRCH CTR
AMSRD ARL VT
F BARTLETT JR MS 266
G FARLEY MS 266
HAMPTON VA 23681-0001

1 FHWA
E MUNLEY
6300 GEORGETOWN PIKE
MCLEAN VA 22101

1 USDOT FEDERAL RAILROAD
M FATEH RDV 31
WASHINGTON DC 20590

1 CYTEC FIBERITE
R DUNNE
1300 REVOLUTION ST
HAVRE DE GRACE MD 21078

1 DIRECTOR
NGIC
IANG TMT
2055 BOULDERS RD
CHARLOTTESVILLE VA
22911-8318

1 3TEX CORP
A BOGDANOVICH
109 MACKENAN DR
CARY NC 27511

NO. OF COPIES ORGANIZATION

1 DIRECTOR
DEFNS INTLLGNC AGCY
TA 5
K CRELLING
WASHINGTON DC 20310

1 COMPOSITE MATERIALS INC
D SHORTT
19105 63 AVE NE
PO BOX 25
ARLINGTON WA 98223

1 JPS GLASS
L CARTER
PO BOX 260
SLATER RD
SLATER SC 29683

1 COMPOSITE MATERIALS INC
R HOLLAND
11 JEWEL CT
ORINDA CA 94563

1 SIMULA
R HUYETT
10016 S 51ST ST
PHOENIX AZ 85044

2 PROTECTION MATERIALS INC
M MILLER
F CRILLEY
14000 NW 58 CT
MIAMI LAKES FL 33014

1 ROM DEV CORP
R O MEARA
136 SWINEBURNE ROW
BRICK MARKET PLACE
NEWPORT RI 02840

1 TEXTRON SYSTEMS
M TREASURE
1449 MIDDLESEX ST
LOWELL MA 01851

1 O GARA HESS & EISENHARDT
M GILLESPIE
9113 LESAINT DR
FAIRFIELD OH 45014

1 CONNEAUGHT INDUSTRIES INC
J SANTOS
PO BOX 1425
COVENTRY RI 02816

NO. OF COPIES ORGANIZATION

1 ARMTEC DEFENSE PRODUCTS
S DYER
85 901 AVE 53
PO BOX 848
COACHELLA CA 92236

3 PACIFIC NORTHWEST LAB
M SMITH
G VAN ARSDALE
R SHIPPELL
PO BOX 999
RICHLAND WA 99352

1 ALLIANT TECHSYSTEMS INC
4700 NATHAN LN N
PLYMOUTH MN 55442-2512

1 APPLIED COMPOSITES
W GRISCH
333 NORTH SIXTH ST
ST CHARLES IL 60174

1 CUSTOM ANALYTICAL
ENG SYS INC
A ALEXANDER
13000 TENSOR LANE NE
FLINTSTONE MD 21530

1 AAI CORP
DR N B MCNELLIS
PO BOX 126
HUNT VALLEY MD 21030-0126

1 PROJECTILE TECHLGY INC
515 GILES ST
HAVRE DE GRACE MD 21078

3 ALLIANT TECHSYSTEMS INC
J CONDON
E LYNAM
J GERHARD
WV01 16 STATE RT 956
PO BOX 210
ROCKET CENTER WV
26726-0210

1 PRATT & WHITNEY
C WATSON
400 MAIN ST MS 114 37
EAST HARTFORD CT 06108

NO. OF COPIES ORGANIZATION

3 NORTHROP GRUMMAN
B IRWIN
K EVANS
D EWART
BLDG 160 DEPT 3700
1100 W HOLLYVALE ST
AZUSA CA 91701

1 BRIGS COMPANY
J BACKOFEN
2668 PETERBOROUGH ST
HERNDON VA 22071-2443

1 ZERNOW TECHL SERVICES
L ZERNOW
425 W BONITA AVE STE 208
SAN DIMAS CA 91773

2 GENERAL DYNAMICS OTS
FLINCHBAUGH DIV
K LINDE
T LYNCH
PO BOX 127
RED LION PA 17356

1 GKN WESTLAND AEROSPACE
D OLDS
450 MURDOCK AVE
MERIDEN CT 06450-8324

1 AEROSPACE CORP
G HAWKINS M4 945
2350 E EL SEGUNDO BLVD
EL SEGUNDO CA 90245

2 CYTEC FIBERITE
M LIN
W WEB
1440 N KRAEMER BLVD
ANAHEIM CA 92806

2 UDLP
G THOMAS
M MACLEAN
PO BOX 58123
SANTA CLARA CA 95052

NO. OF COPIES ORGANIZATION

5 SIKORSKY AIRCRAFT
G JACARUSO
T CARSTENSAN
B KAY
S GARBO MS S330A
J ADELMANN
6900 MAIN ST
PO BOX 9729
STRATFORD CT 06497-9729

2 UDLP
R BRYNSVOLD
P JANKE MS 170
4800 E RIVER RD
MINNEAPOLIS MN 55421-1498

1 LOCKHEED MARTIN
SKUNK WORKS
D FORTNEY
1011 LOCKHEED WAY
PALMDALE CA 93599-2502

1 NORTHRUP GRUMMAN CORP
ELECTRONIC SENSORS
& SYSTEMS DIV
E SCHOCH MS V 16
1745A W NURSERY RD
LINTHICUM MD 21090

1 GDLS DIV
D BARTLE
PO BOX 1901
WARREN MI 48090

1 GDLS
M PASIK
PO BOX 2074
WARREN MI 48090-2074

1 GDLS
MUSKEGON OPER
M SOIMAR
76 GETTY ST
MUSKEGON MI 49442

1 GENERAL DYNAMICS
AMPHIBIOUS SYS
SURVIVABILITY LEAD
G WALKER
991 ANNAPOLIS WAY
WOODBRIDGE VA 22191

NO. OF COPIES ORGANIZATION

5 INST FOR ADVANCED
TECH
H FAIR
I MCNAB
P SULLIVAN
S BLESS
C PERSAD
3925 W BRAKER LN
AUSTIN TX 78759-5316

1 ARROW TECH ASSOC
1233 SHELBURNE RD STE D8
SOUTH BURLINGTON VT
05403-7700

1 SAIC
G CHRYSSOMALLIS
8500 NORMANDALE LAKE BLVD
STE 1610
BLOOMINGTON MN 55437-3828

1 UCLA MANE DEPT ENGR IV
H T HAHN
LOS ANGELES CA 90024-1597

1 UMASS LOWELL
PLASTICS DEPT
N SCHOTT
1 UNIVERSITY AVE
LOWELL MA 01854

1 IIT RSRCH CTR
D ROSE
201 MILL ST
ROME NY 13440-6916

1 MICHIGAN STATE UNIV
MSM DEPT
R AVERILL
3515 EB
EAST LANSING MI 48824-1226

1 PENN STATE UNIV
R S ENGEL
245 HAMMOND BLDG
UNIVERSITY PARK PA 16801

1 PENN STATE UNIV
C BAKIS
212 EARTH ENGR
SCIENCES BLDG
UNIVERSITY PARK PA 16802

NO. OF COPIES ORGANIZATION

1 PURDUE UNIV
SCHOOL OF AERO & ASTRO
C T SUN
W LAFAYETTE IN 47907-1282

1 UNIV OF MAINE
ADV STR & COMP LAB
R LOPEZ ANIDO
5793 AEWC BLDG
ORONO ME 04469-5793

1 JOHNS HOPKINS UNIV
APPLIED PHYSICS LAB
P WIENHOLD
11100 JOHNS HOPKINS RD
LAUREL MD 20723-6099

1 UNIV OF DAYTON
J M WHITNEY
COLLEGE PARK AVE
DAYTON OH 45469-0240

2 UNIV OF DELAWARE
CTR FOR COMPOSITE MTRLS
J GILLESPIE
S ADVANI
201 SPENCER LAB
NEWARK DE 19716

1 MISSISSIPPI STATE UNIV
DEPT OF AEROSPACE ENGRG
A J VIZZINI
MISSISSIPPI STATE MS 39762

1 SOUTHWEST RSRCH INST
ENGR & MATL SCIENCES DIV
J RIEGEL
6220 CULEBRA RD
PO DRAWER 28510
SAN ANTONIO TX 78228-0510

1 DREXEL UNIV
A S D WANG
3141 CHESTNUT ST
PHILADELPHIA PA 19104

1 DEPT OF MTRLS
SCIENCE & ENGRG
UNIV OF ILLINOIS
AT URBANA CHAMPAIGN
J ECONOMY
1304 W GREEN ST 115B
URBANA IL 61801

NO. OF COPIES ORGANIZATION

3 UNIV OF TEXAS AT AUSTIN
CTR FOR ELECTROMECHANICS
J PRICE
A WALLS
J KITZMILLER
10100 BURNET RD
AUSTIN TX 78758-4497

3 DIRECTOR
US ARMY RSRCH LAB
AMSRD ARL WM MB
A FRYDMAN
2800 POWDER MILL RD
ADELPHI MD 20783-1197

1 DEPARTMENT HEAD
US MILITARY ACADEMY
K NYGREN
CIVIL & MECH ENGRG DEPT
WEST POINT NY 10996-1792

1 DIRECTOR
US MILITARY ACADEMY
D BOETTNER
MECH ENGRG DIV
WEST POINT NY 10996-1792

1 US ARMY ARDEC
AMSRD AAR ATD
B MACHAK
BLDG 1
PICATINNY ARSENAL NJ
07806-5000

1 US ARMY ARDEC
AMSRD AAR AEP E
D CARLUCCI
BLDG 94
PICATINNY ARSENAL NJ
07806-5000

10 HAWAII CORROSION LAB
2540 DOLE ST
HOMES HALL RM 302
G HAWTHORN
L HIHARA
HONOLULU HI 96822

NO. OF COPIES ORGANIZATION

2 NORTH DAKOTA STATE UNIV
DEPT OF COATINGS & POLYMERIC MTRLS
G P BIERWAGEN
V J GELLING
1222 9TH ST S
FARGO ND 58105-5516

2 OHIO STATE UNIV
DEPT OF MTRLS SCIENCE & ENGRG
G S FRANKEL
R BUCHEIT
2041 COLLEGE RD WATTS HALL
COLUMBUS OH 43210-1179

1 UNIV OF CALIFORNIA BERKELEY
COLLEGE OF ENGRG
F M DOYLE
308 MCLAUGHLIN HALL NO 1702
BERKELEY CA 94720-1700

1 RENSSELEAR POLYTECHNIC INST
DEPT OF MTRLS ENGRG
D J DUQUETTE
TROY NY 12818

1 THE BOEING COMPANY
DIRECTOR OF MATRLS & PROCESS TECHLGY
D CHONG
2553 134TH AVE SE
BELLEVUE WA 98005

1 UNIV OF VIRGINIA
CTR FOR ELECTROCHEMICAL SCIENCE & ENGRG
DEPT OF MTRLS SCIENCE & ENGRG
J R SCULLY
PO BOX 400745
116 ENGRGS WAY
CHARLOTTESVILLE VA 22904-4745

1 UNIV OF MICHIGAN
DEPT OF MTRLS SCIENCE & ENGRG
G S WAS
H H DOW BLDG
2300 HAYWARD ST
ANN ARBOR MI 48109-2136

1 PENNSYLVANIA STATE UNIV
B SHAW
212 EES BLDG
UNIV PARK PA 16870

NO. OF COPIES ORGANIZATION

1 EXPONENT INC
MECHS & MTRLS DEPT
R M LATANISION
21 STRATHMORE RD
NATICK MA 01760

1 NATIONAL MATERIALS ADVISORY BOARD
M H MOLONEY
500 FIFTH ST NW
MS WS938
WASHINGTON DC 20001

1 USMC
MAINTENANCE CTR ALBANY
S ALLEN
28008 NEWCOMB RD
ALBANY GA 31705

2 AIR FORCE CORROSION PREVENTION & CNTRL OFC
K ANDREWS
MAJ R REED
325 RICHARD RAY BLVD BLDG 165
ROBINS AFB GA 31098-1639

3 US ARMY TACOM TARDEC RDECOM
AMSTA TR E1 MEPS 1267
I C HANDSY
J KOVANDA
A BAZIARI
6501 E 11 MILE RD BLDG 200A
WARREN MI 48397-7738

5 US ARMY RDECOM
AMSRD AMR PS AM
S F CARR
R A HERRON
K BHANSALI
M KANE
A P STEELE
BLDG 7103
REDSTONE ARSENAL AL 35898

1 NASA CORROSION TECHLGY
J CURRAN
MS ASRC 20
KENNEDY SPACE CENTER FL 32899

NO. OF
COPIES ORGANIZATION

1 OUSD (A T & L)
OFC OF CORROSION POLICY &
OVERSIGHT
D J DUNMIRE
2001 N BEAUREGARD ST STE 210
ALEXANDRIA VA 22311

1 OUSD FOR SCIENCE AND TECHLGY
ODDR&E(S &T)
MATRLS & STRUCTURES OFC
L E SLOTER
1777 N KENT ST STE 9030
ARLINGTON VA 22209-2110

3 CONCURRENT TECHNOLOGIES CORP
L GINTERT
R MASON
M SINGLETON
7935 114 TH AVE
LARGO FL 33773

3 US ARMY ERDC
CONSTRUCTION ENGRG RSRCH LAB
V HOCK
A KUMAR
L D STEPHENSON
PO BOX 9005
CHAMPAIGN IL 61826-9005

6 US ARMY ARDEC
ARMY CORROSION OFC
AMSRD AAR AEE P
R ZANOWICZ
J P THEIS
D SKELTON
D SCHMIDT
J ZUNINO
E MCCARTHY
BLDG 60
PICATINNY ARSENAL NJ 07806-5000

1 COMMANDER
NAVSEAAIR
CORROSION RSRCH & ENGRG BR
R HAYS
NSWCCD CODE 613
9500 MACARTHUR BLVD
WEST BETHESDA MD 20817-5700

NO. OF
COPIES ORGANIZATION

2 COMMANDER
NAVAIR
MTRLS COATINGS & CORROSION
C MATZDORF
S SPADAFORA
AIR 4 3 4 BLDG 2188
PATUXENT RIVER MD 20670

2 BATTELLE MEMORIAL INST
NATIONAL SECURITY DIV
MATERIALS AND ENGRG GROUP
W ABBOTT
B HINDIN
505 KING AVE
COLUMBUS OH 43201-2693

ABERDEEN PROVING GROUND

1 US ARMY ATC
CSTE DTC AT AD I
W C FRAZER
400 COLLERAN RD
APG MD 21005-5059

102 DIR USARL
AMSRD ARL CI
AMSRD ARL O AP EG FI
M ADAMSON
AMSRD ARL WM
J SMITH
AMSRD ARL WM B
CHIEF
M ZOLTOSKI
AMSRD ARL WM BA
T KOGLER
D LYON
AMSRD ARL WM BC
J NEWILL
P PLOSTINS
AMSRD ARL WM BD
P CONROY
B FORCH
M LEADORE
C LEVERITT
R LIEB
R PESCE-RODRIGUEZ
B RICE
A ZIELINSKI
AMSRD ARL WM BF
S WILKERSON
AMSRD ARL WM M
J MCCAULEY
S MCKNIGHT
J BEATTY

NO. OF
COPIES ORGANIZATION

AMSRD ARL WM MA
M VANLANDINGHAM
L GHIORSE
AMSRD ARL WM MB
J BENDER
T BOGETTI
J BROWN
L BURTON
K CHO
W DRYSDALE
R EMERSON
D GRAY
D HOPKINS
R KASTE
L KECSKES
H MAUPIN
B POWERS
D SNOHA (10 CPS)
J SOUTH
M STAKER
J SWAB
J TZENG
AMSRD ARL WM MC
R ADLER (10 CPS)
K CHESONIS
J ESCARSEGA
B HART
T JESSEN
J KELLEY
M MAHER
C M MILLER
F PIERCE
B PLACZANKIS
P SMITH
W SPURGEON
S K YOUNG
AMSRD ARL WM MD
B CHEESEMAN
E CHIN
P DEHMER
R DOOLEY
G GAZONAS
S GHIORSE
J LASALVIA
J MONTGOMERY
J SANDS
D SPAGNUOLO
S WALSH
AMSRD ARL WM RP
J BORNSTEIN
E RIGAS
C SHOEMAKER
AMSRD ARL WM SG
R CARTER

NO. OF
COPIES ORGANIZATION

AMSRD ARL WM T
P BAKER
AMSRD ARL WM TA
W BRUCHEY
M BURKINS
B GOOCH
T HAVEL
C HOPPEL
E HORWATH
J RUNYEON
S SCHOENFELD
AMSRD ARL WM TC
R COATES
AMSRD ARL WM TD
D DANDEKAR
M RAFTENBERG
T WEERASOORIYA
AMSRD ARL WM TE
CHIEF
J POWELL

NO. OF
COPIES ORGANIZATION

1 ROYAL INSTITUTE OF TECHNOLOGY
C LEYGRAF
KTH DROTTNING VAG 51
SE 100 STOCKHOLM SWEDEN

INTENTIONALLY LEFT BLANK.